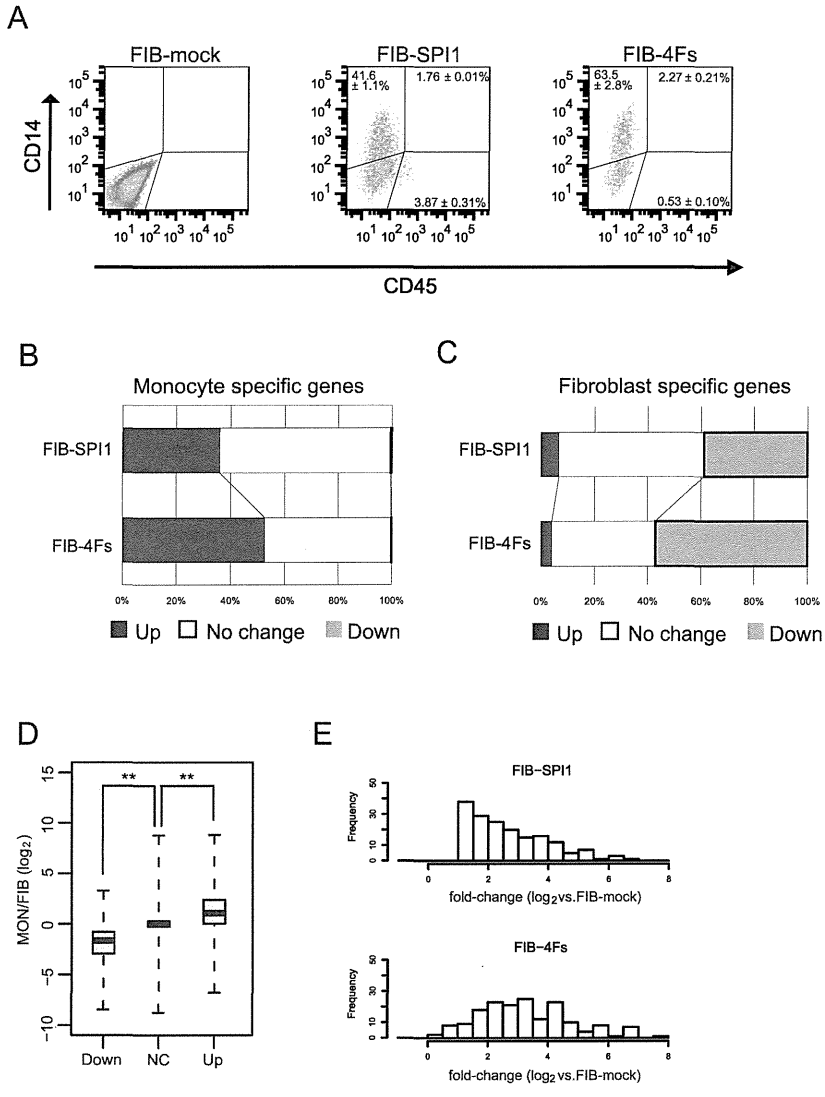

Figure 6. Four TRN-inducersfactors activated wider portion of monocyte TRN than SPI1 alone. (A) Flow cytometric analysis shows expression of CD14 and CD45 and no expression of CD11b in both FIB-SPI1 and FIB-4Fs. All experiments were done in duplicates. (B–C) Bar plots represent the change of up-regulated or down-regulated genes in monocyte specific genes (B) and fibroblast specific genes (C). Total length of the bar represents total number of monocyte specific genes or fibroblast specific genes (100%). The black part is 2^2-fold grater and *P–value*<0.05 (t-test) and gray part represents 2^2-fold less and *P-value*<0.05 (t-test), respectively, comparing to the FIB-mock. (D) All genes were categorized into either Up-regulated (Up), Down-regulated (Down) or No Change (NC) by applying the same cut-off (B–C). Medians for each dataset are indicated by black centerlines, upper quartiles are indicated by upper edges of the box, and lower quartiles are indicated by lower edges of the box. Maximum and minimum values are marked as end of lines extending from the boxes. ** represents *P-value*≤0.01 (Wilcoxson rank sum test). (E) Histogram shows distribution of the fold-change of monocyte specific and up-regulated by *SPI1* (2-fold or greater and *P-value*<0.05 (t-test)). Horizontal axis represents the log value of the fold-change as compare to FIB-mock, and vertical axis represents frequency. Upper histogram is for FIB-SPI1, and lower histogram is for FIB-4Fs.

doi:10.1371/journal.pone.0033474.g006

the translated protein because of post-transcriptional modifications. Therefore, this approach is often beneficial since expression profiling alone may fail to reveal potential candidates that are highly associated to monocytes and their functions. In fact, *STAT5A*, involved in GM-CSF signaling in monocyte differentiation [24], was selected as one of the top 20 TRN-elements by text mining. We also found that *NR4A2*, another element selected by text mining, revealed a large-scale regulation of many core elements possibly a downstream gene of *CEBPA* (Figure 2A and 2B).

In the second step to identify top-line elements, we investigated the relationship among the 20 core TRN elements by perturbation-matrix analysis, which resulted in four most up-stream genes: *SPI1*, *CEBPA*, *MNDA* and *IRF8*. Interestingly, previous reports revealed that *SPI1* and *CEBPA* could convert mouse fibroblasts into macrophage-like cells [25] and mouse neural stem cells to monocyte by *SPI1* alone [26], confirming and supporting our gene selection strategy. In addition, Novershtern et. al recently analyzed the transcriptional circuit in human hematopoiesis and suggested that *SPI1*, *CEBPA* and *MNDA* may function as a monocyte/granulocytes module [27]. Especially, since *MNDA* was not previously characterized as a hematopoietic differentiation related gene, our TRN-based approach can identify the TRN-inducers

Table 2. Expression of monocyte markers.

PROBE_ID	SYMBOL	Average signal intensity				
		Fibroblast	Monocyte	FIB-mock	FIB-SPI1	FIB-4Fs
Up regulated by 4 factors						
ILMN_1740938	APOE	62.19	4001.03	54.93	195.68	5866.35
ILMN_2396444	CD14	104.22	29343.31	106.33	7638.15	22105.52
ILMN_1678833	CCR1	62.83	2602.66	55.52	65.95	166.77
ILMN_1784863	CD36	58.72	8131.47	57.61	60.86	863.00
ILMN_2359907	CD68	550.04	10846.88	458.13	2368.70	3534.46
ILMN_1775501	IL1B	65.38	2448.35	93.12	215.54	9635.38
ILMN_2184373	IL8	216.15	21770.36	606.17	370.42	8960.96
ILMN_1728106	TNF	57.29	950.09	58.29	67.12	231.96
ILMN_1722981	TLR5	57.32	1092.46	53.31	57.93	227.43
ILMN_1654560	TLR6	63.43	1084.65	66.16	86.49	273.07
Unchanged by 4 factors						
ILMN_2413808	CD53	57.44	1629.00	59.68	75.73	72.17
ILMN_2320888	CXCR4	50.97	886.40	45.90	49.31	51.57
ILMN_2261600	FCGR1B	61.86	1044.75	63.55	69.31	72.32
ILMN_1796316	MMP9	55.14	20227.04	54.12	52.63	69.09
ILMN_2392043	SPI1	65.74	828.85	60.00	60.98	65.71
ILMN_1731048	TLR1	59.51	508.74	55.45	68.45	74.31
ILMN_1706217	TLR4	54.60	1077.68	58.77	64.74	94.18

doi:10.1371/journal.pone.0033474.t002

even if it have not been well characterized before, suggesting that it can also be applied to other cellular functions.

SPI1 or *PU.1* has been implicated in transdifferentiation to the myeloid lineage from fibroblasts (in conjunction with *CEBPA* [25]) and adult neural stem cells [26]. In the present study, the monocytic functions were not detected by the transduction of *SPI1* alone, a TF governing most of core TRN elements (Figure 2A and B). The reconstruction of the monocyte TRN by the four identified TRN-inducers revealed major monocyte functions, such as phagocytosis and inflammatory response to LPS. The results suggested that a set of genes associated with cellular functions is not sufficiently regulated by single TF but rather by the concerted action of multiple TFs, a mechanism often observed in cellular differentiation [1]. This mechanism is quite reasonable in terms of cellular robustness, as ectopic expression of single TF does not easily perturb important cellular features. The motif activity of *SPI1* showed an increase in their activity by four TRN-inducers whereas *SPI1* alone could not enhance it sufficiently (Figure 7B), suggesting that although this is directly explained by increase in differential expressional ratio of genes regulated by *SPI1* in FIB-4Fs (Figure 6D), a combinatorial effect may also be critical. In fact, our previous report suggested the combinatorial regulation of *SPI1* and *IRF8* were important factors during monocytic differentiation [28].

A global gene expression analysis and monocyte surface marker analysis revealed that even four factors failed to completely mimic the monocyte expression profile. This indicates that many unknown variables may contribute to the native (endogenous) monocyte TRN. The epigenetic modification may be one of the main reasons as a barrier to prevent the induction of the downstream genes of the monocyte TRN cascade. Indeed, in DNA methylation profiling, the promoter and the enhancer regions of *SPI1* were hyper-methylated in FIB, FIB-SPI1 and FIB-4Fs but not in monocytes (data not shown). While the SPI1 gene is known to be activated by an auto-regulatory feedback loop [27,29], the endogenous expression of *SPI1* was not observed by exogenous transductions (FIB-4Fs and FIB-SPI1). This result strongly suggests that DNA methylation may prevent the SPI1 protein binding to their endogenous *SPI1* regulatory regions.

We designed and generated functional cells from human dermal fibroblasts, reconstructing the monocyte TRN by the identified four factors. In the monocytic lineage, macrophages and dendritic cells are important functional cells for host defense. Macrophages remove foreign invader such as microorganisms or apoptotic cells and dendritic cells have been reported to be applied to cancer therapy as a "dendritic cell vaccine" [30]. Hence, our TRN-based approach to generate functional cells possesses wide possibilities to consider for the cell therapies in the near future.

Materials and Methods

Core TRN Elements Isolation

To profile the gene expression of human $CD14^+$ monocytes (Lonza Japan, Lot no. 080324B) and human neonatal fibroblasts (NB1RGB, Riken Cell Bank), Human WG-6 v3.0 Expression beadschips (Illumina) was used. The probe based signal intensity was normalized by quantile normalization with GenomeStadio softwere (Illumina). To remove un-expressed genes, genes which showed detection *P-value*<0.01 were removed. TFs were extracted based on the human TF list and ranked based on the fold-change. We registered all Illumina microarray data to Gene Expression Omnibus (http://www.ncbi.nlm.nih.gov/geo/) at NCBI (accession number GSE27304). For the text-mining, the abstracts of literatures which have words, "differentiation", "development", or "transformation" were collected from MEDLINE (as of August, 2008) to construct an internal database. Based on this internal database, the number of abstracts in which "monocyte" and "TF

Table 3. Enriched Gene Ontology.

Term	P-Value (Fisher exact test)
Monocytes specific genes	
immune system process	2.00E-56
response to stimulus	5.20E-33
multi-organism process	1.40E-08
locomotion	2.20E-06
death	1.50E-04
biological adhesion	2.10E-04
biological regulation	5.50E-04
FIB-SPI1 up-regulated gene	
immune system process	1.20E-15
multi-organism process	2.30E-08
response to stimulus	3.20E-08
death	1.50E-03
locomotion	2.00E-02
developmental process	2.70E-02
localization	4.40E-02
FIB-4Fs up-regulated genes	
immune system process	2.10E-21
response to stimulus	1.70E-15
multi-organism process	1.60E-11
death	3.30E-05
locomotion	1.70E-03
localization	6.50E-03
establishment of localization	1.40E-02
biological regulation	4.10E-02
FIB-4Fs vs. FIB-SPI1	
immune system process	6.20E-03
multi-organism process	2.10E-02
response to stimulus	2.50E-02
death	3.90E-02

doi:10.1371/journal.pone.0033474.t003

name" were co-occur was counted and ranked. To integrate the two rankings, inverse of the differential expression fold change rank (Rfc) and inverse of the co-occurrence rank (Rco) were added (importance score, IS). Based on the IS, top 20 TFs were isolated as core monocyte TRN elements.

Cells and Cell Culture Conditions

NB1RGB is a normal human skin fibroblast established in Riken Cell Bank (RCB) from male 3 days old neonate was provided from RCB and was cultured in MEM-α (Wako) supplemented with 10% FBS and penicillin/streptomycin (100 U/ml, 100 μg/ml) (Life Technologies). Human CD14 positive monocytes (Lonza, Lot Number; 080324B) were purchased from Takara Bio bio and were cultured in RPMI1640 (Wako) supplemented with 10% FBS, 50 μM 2-mercaptoethanol (Life Technologies), 1 mM sodium pyruvate (Life Technologies), 10 mM HEPES (Life technologies), penicillin/streptomycin (100 U/ml, 100 μg/ml) (Life Technologies). a human embryonic kidney cell line, 293T cells for lentivirus production, were provided from Riken Cell Bank (RCB) and was cultured in Dulbecco's modified Eagle's medium (DMEM) (Wako) supplemented with 10% FBS and penicillin/streptomycin (100 U/ml, 100 μg/ml) (Life Technologies).

Plasmid Construction and Preparation of Viral Vectors

The third generation Self inactivating (SIN) lentiviral vectors, CSII-EF-RfA and CSII-EF-RfA-IRES2-Venus, the packaging plasmids pCAG-HIVgp and pCMV-VSV-G-RSV-Rev were kindly provided by H. Miyoshi (RIKEN BRC). BFP fragment was amplified by using KOD-plus DNA polymerase (TOYOBO) from pREST-BFP (Life Technologies) with the primers (Forward; 5′- AATATGGCCACAACCATGGTGAGCAAGGGCGAGG-AGC -3′, Reverse; 5′- TAGAGTCGCGGCCGCTTACTTG-TACAGCTCGTCCATGCCGAG -3′), and Bsd fragment was amplified by the KOD-plus polymerase from pCMV-Bsd (Life Technologies) with the primers (Forward; 5′- AATATGGCCA-CAACCATGGCCAAGCCTTTGTCTCAAGAAG-3′, Reverse; 5′- TAGAGTCGCGGCCGCTTAGCCCTCCCACACATAA-CCAG-3′). These PCR products were joined with the linearized pIRES2 plasmid which was generated with the primers (Forward; 5′-GCGGCCGCGACTCTAGATCATAATC-3′, Reverse; 5′-GGTTGTGGCCATATTATCATCGTGTTTTTC-3′) to amplify the whole sequence of pIRES2-DsRed-Express2 (Clontech) except the DsRed-Express2 sequence by using the In-Fusion technology, resulting pIRES2-BFP, and pIRES2-Bsd. IRES2-BFP, IRES2-DsRed-Express2, and IRES2-Bsd fragments were amplified from these pIRES2 plasmids including the original pIRES2-DsRed-Express2 with the following primers ((IRES2-BFP) Forward; 5′-CCGCGGATCCTCTAGAGCTAGCGCTACCGG-ACTCAGATC-3′, Reverse; 5′-CGATGTTAACTCTAGAT-TACTTGTACAGCTCGTCCATGCCGAG-3′, (IRES2-DsRed--Express2) Forward; 5′-CCGCGGATCCTCTAGAGCTAGCGC-TACCGGACTCAGATC-3′, Reverse; 5′-CGATGTTAACTC-TAGACTACTGGAACAGGTGGTGGCG-3′, (IRES2-Bsd) Forward; 5′-CCGCGGATCCTCTAGAGCTAGCGCTACCGGA-CTCAGATC-3′, Reverse; 5′-CGATGTTAACTCTAGAT-TAGCCCTCCCACACATAACCAG-3′). These fragments were inserted into Xba I site of CSII-EF-RfA, resulting CSII-EF-RfA-IRES2-BFP (DsRed-express2, or Bsd).

Human transcription factor genes were sub-cloned from the entry clones into CSII-EF1α-RfA-IRES2 lentiviral expression vectors.

Lentivirus Preparation

293T cells were seeded on to a poly-L-lysine courted 10 cm dish (BD) 24 hours before transfection at 4×10^6 cells in 8 ml Opti-MEM glutaMAX (Life Technologies) supplemented with 5% FBS. One hour before transfection, the medium was replaced to fresh Opti-MEM glutaMAX medium (5% FBS, 25 μM chloroquine). The lentiviral expression vector (17 μg) and the packaging constructs, pCMV-VSV-G-RSV-Rev (10 μg) and pCAG-HIVgp (10 μg) were mixed with 1200 μl Opti-MEM (Life Technologies). Then 100 μl FuGENE HD Transfection reagent (Roche) was added to the mixture and the solution was vortex briefly, incubated for 15 min at RT. The Transfection complex was added dropwise onto the 293T cell culture. Medium was replaced to fresh Opti-MEM 24 hours after transfection. Virus containing supernatant was collected 24 hours after the medium replacement and stored at 4°C, fresh 8 ml Opti-MEM was add to the dish. The supernatant was collected 24 hours after the first medium collection and combined with the supernatant collected at first collection. Combined virus containing supernatant was filtered with 0.45 μm syringe filter (NIPPON Genetics). Filtered supernatant was ultra-centrifuged at 50000 g (19400 rpm in a Beckman

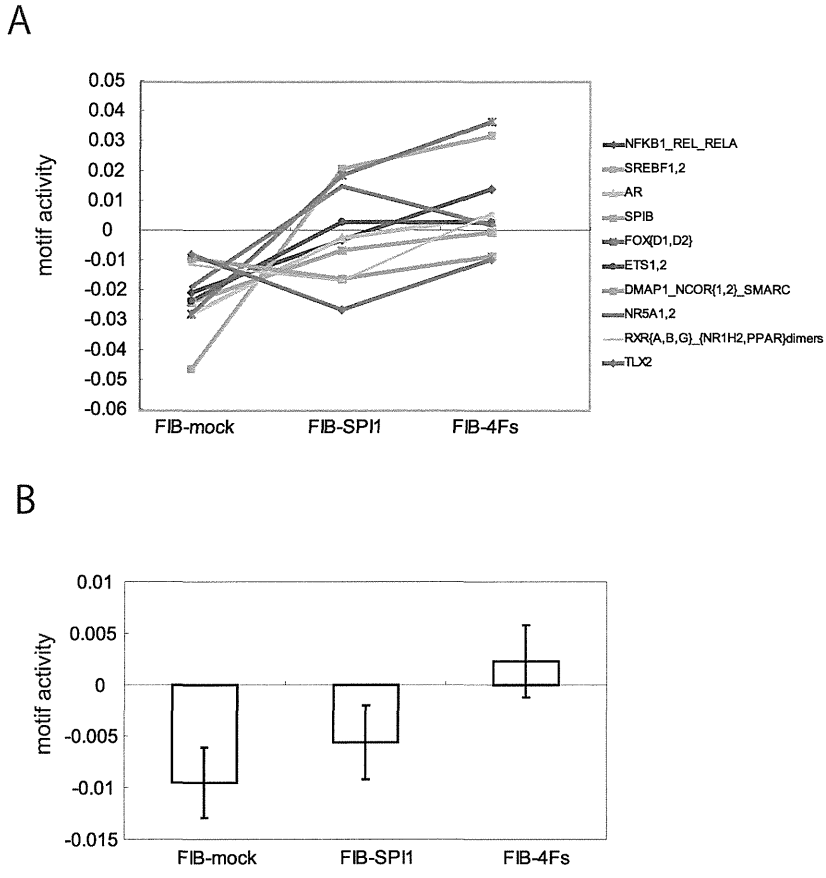

Figure 7. Motif activity revealed reconstructed monocyte TRN. (A) The activity of 10 monocyte-associated motifs were shown as a line chart in FIB-mock, FIB-SPI1, and FIB-4Fs. Vertical axis represents the motif activity. (B) SPI1 motif activity was shown as bar plot. Each bar represent an average of biological replicates and error bar represent s.d. (n = 3).
doi:10.1371/journal.pone.0033474.g007

SW28 rotor) for two hours at 20°C. Pelletized virus particles were resuspended in 100 µl HBSS and stored at −80°C until used.

Lentivirus Titration

Concentrated SIN lentivirus vector was diluted 300 times with HBSS. Lentivirus RNA was extracted by using NucleoSpin® RNA Virus (MACHEREY-NAGEL) according the manufacture's instruction. Elution was done with 50 µl Elution buffer and extracted viral RNA was treated with 4 µl DNase I (Takara Bio) for 30 min at 37°C. One-step qRT-PCR was performed by using One Step SYBR PrimeScript RT-PCR Kit II (Takara Bio) with the primers (Forward; 5′-CCGTTGTCAGGCAACGTG-3′, Reverse; 5′-AGCTGACAGGTGGTGGCAAT-3′) according the manufacture's instruction. The virus titer was calculated from the Ct value based on that of the control virus whose infectivity was preliminary determined via flow cytometry.

Flow Cytometry

Flow cytometry and cell sorting were performed with a FACSAria II SORP (BD Bioscience) and analyzed with FlowJo software. For the surface marker analysis, 1×10^6 cells were detached with 0. 5 mM EDTA/PBS and resuspended in 1 ml washing buffer (PBS supplemented 2% FBS), incubated for 1 hour at 4°C with Alexafluor700 conjugated anti human CD14 antibody (Biolegend, Cat#; 325614, Lot#; B112226), and Alexafluor647 conjugated anti human CD45 antiybody (Biolegend, Cat#; 304018, Lot#; B116410). The cells were washed twice with the washing buffer and resuspended in 1 ml washing buffer. The combination of excitation laser and detector were Red (633 nm)-660/20 for Alexafluor647, and Red (633 nm) - 730/45 for Alexafluor700. All experiments were done in duplicates.

Gene Transduction and Cell Selection

Human fibroblasts were seeded onto a 100 mm dish at 4×10^5 cells with MEM-α 24 hours before infection. The medium was changed to 8 µg/ml polybrene containing medium and added lentivirus vectors at 5 or 10 MOI. The medium was replaced to fresh medium 24 hours after the infection. Cell sorting was achieved by FACS Aria II SORP. For the matrix over expression analysis, cells were cultured eight days after the gene transduction. Cells were detached and resuspended in washing buffer at 1×10^6 cells/ml, sorted based on Venus fluorescence. For the combinatorial four factors transduction, IRF8-BFP and MNDA-Bsd were transduced into the fibroblasts and six days after the transduction, *MNDA* transduced cells were selected by adding blasticidine at the final concentration of 8 µg/ml for 10 days. After the blasticidine selection, *IRF8* transduced cells were sorted based on BFP fluorescence. The sorted cells were transduced with SPI1-DsRed and CEBPA-Venus. Eight days after the second transduction, the cells were sorted based on both DsRed and Venus fluorescence.

The combination of excitation laser and detector were Violet (405 nm)-450/40 for BFP, Blue (488 nm)-530/30 for Venus, and Blue (488 nm)-610/20 for DsRed-Express2,

Microarray Analysis

Total RNAs were extracted with FastPure RNA kit (Takara Bio) and observed their quality by using an Agilent 2100 Bioanalyzer. From 500 ng of the total RNA, biotinylated cRNA were produced with the Illumina RNA Amplification Kit (Ambion) according to the manufacturer's instructions. The concentration of the cRNA solution was determined by spectrophotometric measurement, and the size distribution of cRNA was evaluated using the Agilent 2100 Bioanalyzer. cRNA was hybridized using Human WG-6 v3.0 Expression beadschips (Illumina) according to the manufacturer's instructions. Hybridization was done in triplicate, and the signal intensity of each data set was normalized by quantile normalization. The data were analyzed with BeadStudio (Illumina), GeneSpring, and R. We registered all Illumina microarray data to Gene Expression Omnibus (http://www.ncbi.nlm.nih.gov/geo/) at NCBI (accession number GSE27304).

Quantitative Reverse Transcription-Polymerase Chain Reaction (qRT-PCR)

Total RNA was extracted by using FastPure RNA kit (Takara Bio). Reverse transcription of total RNA was achieved with PrimeScript^{TM} Reverse Transcriptase (Takara Bio) and random hexamers in accordance with the manufacturer's protocol. Glyceraldehyde-3-phosphate dehydrogenase (GAPDH) mRNA was used as a control (primers *5′GAAGGTGAAGGTCGGAGT-3′* and *5′GAAGATGGTGATGGGATTTC-3′*) for data normalization. The PCR primers used for each gene in this analysis are given in Table S3. PCR amplification was performed on an ABI PRISM® 7500 Sequence Detection System (Applied Biosystems). For amplification, SYBR Premix Ex *Taq*^{TM} II (Takara Bio) was used as instructed in the manual. The PCR conditions were an initial step of 10 seconds at 95°C, followed by 40 cycles of 3 sec at 95°C and 20 sec at 62.5°C. Changes of gene expression were determined using the $2^{-\Delta\Delta Ct}$ method.

Flow Cytometric Phagocytosis Assay

Cells were incubated at 37°C at 5% CO_2 with 0.002v/v% red fluorescent latex beads (SIGMA, diameter; 2.0 μm) for 2, 4, and 6 hours. Cells were washed five times with fresh medium and resuspended in 2% FBS-PBS to analyze the beads ingestion using the flow cytometer. The analysis was done in triplicates.

Confocal Microscopy Imaging of Phagocytosis

Cells were incubated at 37°C, 5% CO_2 with 0.001v/v% red fluorescent latex beads (SIGMA, diameter; 2.0 μm) for four hours in eight well Lab-Tek glass chamber slides (Nunc). The cell membrane was stained with DiD (Life technologies) and the nucleus was stained with Hoechst33343 (Life technologies), followed by confocal microscopy imaging (Leica, DMI4000B).

Inflammatory Response Analysis

FIB-mock, FIB-SPI1, and FIB-4Fs were treated with LPS (sigma) at the final concentration of 10 μg/ml for 24 hours. The LPS treated and untreated cells were collected and their RNA was extracted. Extracted RNAs were performed qRT-PCR as described above for *TNF*, *IL6*, *IL1A*, *IL1B*, *IL8*, *CCL2*, *CXCL10* and *IFNB1*. The primer sequences were shown in Table S3. The fold-change of those genes was computed comparing with LPS untreated cells.

Proteome profiler protein array

FIB-mock and FIB-4Fs were treated with LPS as described above on 6-well plates. The culture media were collected from the LPS-treated and -untreated wells after 16 hours. From one ml of the collected media, secreted cytokines were measured using Proteome Profiler Array Human Cytokine Array Panel A (R & D Systems) and ECL Prime Detection Reagent (GE Healthcare), following the manufacture's instruction. The chemiluminescence was detected by LAS-3000 (Fujifilm). The detected pixel density was analyzed by Multi Gauge software (Fujifilm).

Chemotaxis activity assay

FIB-mock and FIB-4Fs were plated to trans-well inserts at 1×10^5 cells and cultured for 24 hours with MEM-α (10% FBS). The cells were washed and cultured with Chemotaxis Assay Buffer (HBSS, 0.1% BSA). Human recombinant CCL2 (Sigma) were added to the companion plate (lower chamber) at the final concentration of 5 μM and cultured for additional 16 hours in 37°C CO_2 incubator. The cells were stained with Calcein-AM (Life technologies) and the fluorescence intensity of the transwell inserts were measured using the ARVO plate reader system (PerkinElmer).

Motif Activity Analysis

The motif activities were calculated as described previously [1] using position-weight matrices obtained from Swiss Regulon [31]. We searched for transcription factor binding site using the MotEvo algorithm [32] in the −300 to +100 base pair region with respect to the 5′ end of the Refseq transcript associated with each microarray probe, using a prior probability of 10^{-5}.

Supporting Information

Figure S1 (A) Lentiviral expression vectors. (B) Strategy to collect multiple TFs transduced cells.
(EPS)

Figure S2 Heatmap representation of relative expressions to GAPDH. Higher relative expression is depicted as light green color. The value of each relative expression is the average of biological replicates (n = 3).
(EPS)

Table S1 Full result of text-mining.
(PDF)

Table S2 Human transcription factor list.
(PDF)

Table S3 Primer sequences for qRT-PCR.
(PDF)

Acknowledgments

We thank Hiroyuki Miyoshi for provision of Lentivirus expression and packaging plasmids; Toshitada Takemori, Hiroshi Kawamoto, Hiroto Tanaka, for helpful advice and useful suggestions; Mami Kishima-ikegami, Noriko Ninomiya-Fukuda, Chizuru Suzuki, and Ayumi Ogawa for experimental support. We are also grateful to the members of RIKEN Omics Science Center.

Author Contributions

Conceived and designed the experiments: TS Y. Hasegawa Y. Hayashizaki HS. Performed the experiments: TS MNI HYO SSH AK CS. Analyzed the data: TS JS MDH. Wrote the paper: TS JWS HS.

References

1. Suzuki H, Forrest AR, van Nimwegen E, Daub CO, Balwierz PJ, et al. (2009) The transcriptional network that controls growth arrest and differentiation in a human myeloid leukemia cell line. Nat Genet 41: 553–562.
2. Wenzlau JM, Juhl K, Yu L, Moua O, Sarkar SA, et al. (2007) The cation efflux transporter ZnT8 (Slc30A8) is a major autoantigen in human type 1 diabetes. Proc Natl Acad Sci U S A 104: 17040–17045.
3. Takahashi K, Yamanaka S (2006) Induction of pluripotent stem cells from mouse embryonic and adult fibroblast cultures by defined factors. Cell 126: 663–676.
4. Takahashi K, Tanabe K, Ohnuki M, Narita M, Ichisaka T, et al. (2007) Induction of pluripotent stem cells from adult human fibroblasts by defined factors. Cell 131: 861–872.
5. Zhou Q, Brown J, Kanarek A, Rajagopal J, Melton DA (2008) In vivo reprogramming of adult pancreatic exocrine cells to beta-cells. Nature 455: 627–632.
6. Vierbuchen T, Ostermeier A, Pang ZP, Kokubu Y, Sudhof TC, et al. (2010) Direct conversion of fibroblasts to functional neurons by defined factors. Nature 463: 1035–1041.
7. Ieda M, Fu JD, Delgado-Olguin P, Vedantham V, Hayashi Y, et al. (2010) Direct reprogramming of fibroblasts into functional cardiomyocytes by defined factors. Cell 142: 375–386.
8. Szabo E, Rampalli S, Risueno RM, Schnerch A, Mitchell R, et al. (2010) Direct conversion of human fibroblasts to multilineage blood progenitors. Nature 468: 521–526.
9. Trefzer U, Walden P (2003) Hybrid-cell vaccines for cancer immune therapy. Mol Biotechnol 25: 63–69.
10. de Hoon M, Hayashizaki Y (2008) Deep cap analysis gene expression (CAGE): genome-wide identification of promoters, quantification of their expression, and network inference. Biotechniques 44: 627–628, 630, 632.
11. Tomaru Y, Nakanishi M, Miura H, Kimura Y, Ohkawa H, et al. (2009) Identification of an inter-transcription factor regulatory network in human hepatoma cells by Matrix RNAi. Nucleic Acids Res 37: 1049–1060.
12. Melief CJ (2008) Cancer immunotherapy by dendritic cells. Immunity 29: 372–383.
13. Bhardwaj N, Kim PM, Gerstein MB (2010) Rewiring of transcriptional regulatory networks: hierarchy, rather than connectivity, better reflects the importance of regulators. Sci Signal 3: ra79.
14. Ravasi T, Suzuki H, Cannistraci CV, Katayama S, Bajic VB, et al. (2010) An atlas of combinatorial transcriptional regulation in mouse and man. Cell 140: 744–752.
15. Rosa A, Ballarino M, Sorrentino A, Sthandier O, De Angelis FG, et al. (2007) The interplay between the master transcription factor PU.1 and miR-424 regulates human monocyte/macrophage differentiation. Proc Natl Acad Sci U S A 104: 19849–19854.
16. Kedzierska K, Azzam R, Ellery P, Mak J, Jaworowski A, et al. (2003) Defective phagocytosis by human monocyte/macrophages following HIV-1 infection: underlying mechanisms and modulation by adjunctive cytokine therapy. J Clin Virol 26: 247–263.
17. Mosser DM, Edwards JP (2008) Exploring the full spectrum of macrophage activation. Nat Rev Immunol 8: 958–969.
18. Allen TD, Schor SL (1983) The contraction of collagen matrices by dermal fibroblasts. J Ultrastruct Res 83: 205–219.
19. Yamana J, Santos L, Morand E (2009) Enhanced induction of LPS-induced fibroblast MCP-1 by interferon-gamma: involvement of JNK and MAPK phosphatase-1. Cell Immunol 255: 26–32.
20. Arlein WJ, Shearer JD, Caldwell MD (1998) Continuity between wound macrophage and fibroblast phenotype: analysis of wound fibroblast phagocytosis. Am J Physiol 275: R1041–1048.
21. Huang da W, Sherman BT, Lempicki RA (2009) Systematic and integrative analysis of large gene lists using DAVID bioinformatics resources. Nat Protoc 4: 44–57.
22. Freytag SO, Geddes TJ (1992) Reciprocal regulation of adipogenesis by Myc and C/EBP alpha. Science 256: 379–382.
23. Sato Y, Miyake K, Kaneoka H, Iijima S (2006) Sumoylation of CCAAT/enhancer-binding protein alpha and its functional roles in hepatocyte differentiation. J Biol Chem 281: 21629–21639.
24. Lehtonen A, Matikainen S, Miettinen M, Julkunen I (2002) Granulocyte-macrophage colony-stimulating factor (GM-CSF)-induced STAT5 activation and target-gene expression during human monocyte/macrophage differentiation. J Leukoc Biol 71: 511–519.
25. Feng R, Desbordes SC, Xie H, Tillo ES, Pixley F, et al. (2008) PU.1 and C/EBPalpha/beta convert fibroblasts into macrophage-like cells. Proc Natl Acad Sci U S A 105: 6057–6062.
26. Forsberg M, Carlen M, Meletis K, Yeung MS, Barnabe-Heider F, et al. (2010) Efficient reprogramming of adult neural stem cells to monocytes by ectopic expression of a single gene. Proc Natl Acad Sci U S A 107: 14657–14661.
27. Novershtern N, Subramanian A, Lawton LN, Mak RH, Haining WN, et al. (2011) Densely interconnected transcriptional circuits control cell states in human hematopoiesis. Cell 144: 296–309.
28. Kubosaki A, Lindgren G, Tagami M, Simon C, Tomaru Y, et al. (2010) The combination of gene perturbation assay and ChIP-chip reveals functional direct target genes for IRF8 in THP-1 cells. Mol Immunol 47: 2295–2302.
29. Okuno Y, Huang G, Rosenbauer F, Evans EK, Radomska HS, et al. (2005) Potential autoregulation of transcription factor PU.1 by an upstream regulatory element. Mol Cell Biol 25: 2832–2845.
30. Steele JC, Rao A, Marsden JR, Armstrong CJ, Berhane S, et al. (2011) Phase I/II trial of a dendritic cell vaccine transfected with DNA encoding melan A and gp100 for patients with metastatic melanoma. Gene Ther.
31. Pachkov M, Erb I, Molina N, van Nimwegen E (2007) SwissRegulon: a database of genome-wide annotations of regulatory sites. Nucleic Acids Res 35: D127–131.
32. van Nimwegen E (2007) Finding regulatory elements and regulatory motifs: a general probabilistic framework. BMC Bioinformatics 8 Suppl 6: S4.

Published online 8 August 2012

Nucleic Acids Research, 2012, Vol. 40, No. 21 ***e165***
doi:10.1093/nar/gks732

Establishment of single-cell screening system for the rapid identification of transcriptional modulators involved in direct cell reprogramming

Jay W. Shin, Takahiro Suzuki, Noriko Ninomiya, Mami Kishima, Yuki Hasegawa, Atsutaka Kubosaki, Haruka Yabukami, Yoshihide Hayashizaki and Harukazu Suzuki*

Omics Science Center, RIKEN Yokohama, 1-7-22 Suehiro-cho Tsurumi-ku, Yokohama, Kanagawa 230-0045, Japan

Received April 16, 2012; Revised June 21, 2012; Accepted July 9, 2012

ABSTRACT

Combinatorial interactions of transcription modulators are critical to regulate cell-specific expression and to drive direct cell reprogramming (e.g. trans-differentiation). However, the identification of key transcription modulators from myriad of candidate genes is laborious and time consuming. To rapidly identify key regulatory factors involved in direct cell reprogramming, we established a multiplex single-cell screening system using a fibroblast-to-monocyte transition model. The system implements a single-cell 'shotgun-transduction' strategy followed by nested-single-cell-polymerase chain reaction (Nesc-PCR) gene expression analysis. To demonstrate this, we simultaneously transduced 18 monocyte-enriched transcription modulators in fibroblasts followed by selection of single cells expressing monocyte-specific CD14 and HLA-DR cell-surface markers from a heterogeneous population. Highly multiplex Nesc-PCR expression analysis revealed a variety of gene combinations with a significant enrichment of SPI1 (86/86) and a novel transcriptional modulator, HCLS1 (76/86), in the $CD14^{+}$/$HLA\text{-}DR^{+}$ single cells. We could further demonstrate the synergistic role of HCLS1 in regulating monocyte-specific gene expressions and phagocytosis in dermal fibroblasts in the presence of SPI1. This study establishes a platform for a multiplex single-cell screening of combinatorial transcription modulators to drive any direct cell reprogramming.

INTRODUCTION

A defined combination of transcription modulators is key to target-directed cell reprogramming or trans-differentiation. Retro/lentiviruses have enabled genetic approaches in cultured primary cells to ectopically express genes of interest (1–6). Viral screens using focused overexpression libraries can identify putative reprogramming factors, for example, by identifying a defined set of transcription factors that are selectively required to induce pluripotent stem cells (2–4,7) or trans-differentiate from mature somatic cell into another mature somatic cell (1,8–11). Despite the power of viral technologies, pooled screens for cell reprogramming have generally adopted a one-by-one elimination approach or testing for exhaustive combinations and interrogating phenotypes in cell culture from transgenic mice (1,3,10) and/or aberrantly cloned cell lines (12). These approaches require both considerable specialty and a substantial investment in time.

We therefore implemented a rapid and direct approach by allowing multiple viruses to infect at random and identify specific viral transcripts that give rise to target-specific expressions at a single cell level. Our focus was identifying essential interplay of transcription 'modulating' factors (TMs) through lentivirus that were selectively expressed at a single-cell level. This type of screen holds promise for discovery of novel combination of TMs for regenerative medicine (1,13) or for any screening assay, which requires selectable phenotype such as biomarkers and cancer stem cells (14,15).

We and others previously described that the genetic interactions is key to defining the transcription regulatory network of human monocytes (16,17). We thus hypothesized that introducing the transcriptional network of

*To whom correspondence should be addressed. Tel: +81 45 503 9222; Fax: +81 45 503 9216; Email: harukazu@gsc.riken.jp

monocytes into fibroblasts would promote trans-differentiation into functional monocytes characterized by the expression of both CD14 and HLA-DR surface antigens. In this study, we transduced a pool of 18 monocyte-enriched transcription modulators into human dermal fibroblasts and isolated CD14 and HLA-DR-positive single cells after 2 weeks. A highly multiplex nested-single-cell-polymerase chain reaction (Nesc-PCR) analysis showed heterogeneous infection patterns but revealed significant enrichments of SPI1 and HCLS1 transcripts when selected for monocyte markers. On the basis of our single-cell screening method, we further demonstrate that SPI1 promoted and HCLS1 enhanced marker expressions and function specific to monocytes in dermal fibroblasts.

MATERIALS AND METHODS

Complementary DNA and virus preparation

Gateway-compatible human full-length complementary DNA (cDNA) entry clones derived from RIKEN BRC clone bank [http://www.brc.riken.jp/ (23 July 2012, date last accessed)], Invitrogen (Carlsbad, CA, USA) and OpenBiosystems (Huntsville, AL, USA) were recombined into 150 ng of pENTR lentivirus vector (CSII-EF-RfA-IRES2-VENUS; Supplementary Figure S1) overnight at room temperature using Gateway LR clonaseII enzyme mix (Invitrogen). After 2 h of Protease K treatment at 55°C, recombined plasmids were transformed into OneShot® *Stbl3* competent *Escherichia coli* (Invitrogen) following manufacturer's protocol. Plasmids derived from single colony were expanded and purified using PureYield Plasmid Midiprep System (Promega). For every 8.5 μg of the plasmid, 5 μg of HIV-gp and 5 μg of VSV envelop genes were co-transfected onto 4×10^6 293T cells (prepared the day before at 37°C, 10% CO_2) using FuGeneHD (Roche) in OPTI-MEM (WAKO) medium containing 5% FBS at 37°C 5% CO_2. Between 24 h and 72 h of incubation, supernatant-containing virus were collected and centrifuged at 19 400rpm for 2 h at 20°C. The pallet was then dissolved in 100 μl HBSS buffer (WAKO), followed by titer check and stored at −80°C freezer for later use.

Virus titer check

One microliter of concentrated virus from the previous step was serially diluted (1:1000, 1:3000, 1:9000, 1:27 000 and 1:36 000) in MEM-α containing 10% FBS/L-glutamine/antibiotics (WAKO) and transduced onto 3000 of 293 T cells seeded in a black clear-bottom 96-well plate (BD) for 3 days. The nucleus was stained using Hoechst (Invitrogen) for 30 min at 37°C 5% CO_2, and the plate was subjected to Cellomics ArrayScan XTi Reader (ThermoScientific) for image analysis. FITC and Hoechst filters were used to detect Yellow Fluorescent Protein derivative (Venus) and nuclear staining, respectively, at 10× magnification, and 10 images were taken per each well. Cellomics bio-application protocol 'SpotDetector' was used to segment Hoechst+ nucleus and to count Venus overlapping cells. The titer was calculated by

$$\text{Titer (c.f.u)} = ([\text{dilution factor} \times \%\ \text{of Venus+cells} \times \text{initial cell number} \times \text{volume per well}]/\text{volume of concentrated virus}).$$

Cell culture and virus transduction

Human $CD14^+$ primary monocytes were purchased from Lonza, and THP1 cells (16) were cultured in monocyte medium containing RPMI1400 (WAKO) containing 10% FBS/5M HEPES/2.5M sodium pyruvate/3.4 μg β-mercaptoethanol/L-glutamine/antibiotics (GIBCO). Human dermal fibroblasts (Passages 5–8) were purchased from RIKEN BRC and prepared at 5×10^4 cells in culture media: MEM-α containing 10% FBS/L-glutamine/antibiotic (WAKO) at 37°C 5% CO_2 1 day before virus transduction. A total of 10 multiplicity of infection (MOI, 0.55 MOI per TM) were pooled into 3 ml of culture media containing 80 mg/ml of Polybrene (SIGMA) to increase transduction efficiency. The virus was transduced and incubated for 2 weeks in 37°C 5% CO_2 with MEM-α containing 10% FBS/L-glutamine/antibiotic in the period of first 5 days and in the monocyte medium for the remaining 9 days.

Immunostaining and cell sorting

Two weeks post-virus transduction, cells were detached using Accutase and stained with human anti-CD14/AlexaFluora700 (BioLegend) and human anti-HLA-DR/APC (BD) antibodies for 30 min in ice. Fluorescence-activated cell sorting (FACS) analysis was performed on BD FACS Aria II (BD) for sorting $Venus^+/CD14^+/HLA\text{-}DR^+$ single cells. To ensure a successful capture of single cells, we verified the cell-sorting accuracy before every experiment by observing the cells under a fluorescent microscope to confirm the alignment (center of the well) and to detect a single cell body. We detected 72 ± 10% positive single cells. Thereafter, single cells were sorted directly into 96-well plate containing the pre-amplification mixture. Pre-amplified samples positive for ACTB expression were used for the subsequent analysis.

Candidate gene extraction

Illumina Human WG-6 version 3.0 microarrays were used to analyze differentially expressed transcripts between human dermal fibroblasts and CD14+ monocytes (18) (GSE27304). After quantile normalization, top 20 most differentially expressed transcripts annotated as 'regulation of transcription' [based on Gene Ontology (19)] in monocytes when compared with fibroblasts were selected for lentivirus production (Student's *t*-test: P value < 0.001). The viral transcripts, GAS7 and EGR2, could not be detected using Nesc-PCR; hence, they were removed from the virus pool.

Nested-single-cell PCR

The primer mix for pre-amplification consisted of 20 μM of sense primers targeting ORF region of each gene (total

36) plus 100 μM of Attb2 anti-sense primer or 20 μM of anti-sense primer for endogenous transcripts for primary fibroblasts and monocytes. The primer mixture is further diluted to 200 nM and mixed with OneStep qRT-PCR 2 × Reaction Mix, SuperScriptIII RT/Platinum TaqMix, RNAse OUT (Invitrogen) and DNAse/RNase-free distilled water (GIBCO) to total volume of 9 μl per reaction. After single-cell sorting, the samples were incubated at 55°C for 25 min, 95°C for 2 min and 18 cycles of 95°C for 15 s and 60°C for 4 min. The final samples were diluted 1:5 with DNase/RNase-free water and stored in −20°C for later use. Primer mixture for PCR amplification consisted of 20 μM of both sense and antisense primer pairs targeting ORF region of each gene plus 0.3 μM of UPL probe for specificity (ROCHE). Additional 2× assay loading reagent (Fluidigm) and water were added to adjust final volume of 5 μl per reaction. Diluted pre-amplified cDNA (1.25 μl) is mixed with 2× FastStart Universal Probe Master (ROX; ROCHE) and 20× GE Sample loading reagent (Fluidigm) and water to final volume of 5 μl per reaction. The primer mix and the sample mix were loaded onto 48.48 Dynamic Array (Fluidigm) and primed and mixed using the MX IFC controller (Fludigm). The dynamic array was further subjected to BioMark Array System (Fluidigm) at 95°C for 10 min and 40 cycles of 95°C for 15 min and 60°C for 1 min.

Single-cell data analysis and statistics

Expression data from BioMark (Fluidigm) were processed in R Bioconductor (20). To illustrate gene expression and for statistical analyzes, we first set all *Ct* values >35 to 35 and inversed the expression by subtracting the values by 35. To test the statistical significance of marker enrichment analysis, we performed chi-square test to compare observed data (detected number of exogenous TM) with data we would expect to obtain (marker+ cells and marker − cells). The data are presented in terms of percentages.

qRT-PCR

Reverse transcription of total ribonucleic acid (RNA) was achieved with PrimeScript™ Reverse Transcriptase (Takara) and random hexamers in accordance with the manufacturer's protocol. Beta actin (ACTB) messenger RNA was used as a control for data normalization. The PCR primers used for each gene in this analysis are provided in Supplementary Table S2. PCR amplification was performed on an ABI PRISM® 7500 Sequence Detection System (Applied Biosystems). For amplification, SYBR Premix Ex Taq™ II (Takara) was used as instructed in the manual. Changes of gene expression were determined using the $2-^{\Delta\Delta Ct}$ method.

Phagocytosis assay

Combinations of vector control, SPI1 and HCLS1, were transduced onto human dermal fibroblasts seeded at 5000 cells in a black clear bottom 96-well plate for a period of 20 days in RPMI1400 (WAKO) containing 10% FBS/5 M HEPES/2.5 M sodium pyruvate/3.4 μg β-mercaptoethanol/L-glutamine/antibiotics (GIBCO) at 37°C 5% CO_2. Each plate contained six replicate wells of the same condition. The experiment was performed two independent times. One vial (2 mg) of the pHrodo BioParticles fluorescent particles (Invitrogen) were diluted in 4 ml of uptake buffer consisting of HBSS (WAKO), 20 mM HEPES, pH 7.4 and replaced the culture medium with 100 μl of the prepared pHrodo BioParticles suspension. The plate was incubated in 37°C 5% CO_2 for 7 h, and cells were stained with Hoechst (Invitrogen) for 1 h at 37°C 5% CO_2. The images were taken using the Leica XT microscope (Leica) and quantified using Cellomics ArrayScan XTi Reader (ThermoScientific).

siRNA transfection and RNA extraction

Reverse transfection of 1×10^6 THP1 cells in each 60-mm cell culture dish was performed with 20 nM of each stealth negative control siRNA, SPI1 siRNA (Stealth RNAi: UG GUGCCCUAUGACACGGAUCUAUA) or HCLS1 siRNA (Silencer® Select, Invitrogen; siRNA ID s6484) in Opti-MEM and Lipofectamine 2000 (Invitrogen), according to the manufacturer's instructions. Total RNA was extracted 48 h after transfection using miRNAeasy kit (Qiagen) according to manufacturer's instructions.

RESULTS

Single-cell screening system

To rapidly screen for TMs involved in the direct monocyte specification, we designed an experimental workflow that integrates lentivirus technology (5,6), FACS and single-cell profiling analysis (21–23) (Figure 1). Human primary dermal fibroblasts were simultaneously transduced with a lentivirus pool of 18 monocyte-enriched TMs, selected based on gene-specific expression in primary CD14+ monocytes when compared with dermal fibroblasts (Supplementary Table S1, see Section 'Materials and Methods'). The stochastic nature of the virus infection allows for a mixed combination of TMs to be expressed per infected single cell, giving rise to target-specific expressions from a sub-population that accompanies the defined combination of monocyte-specifying TMs. A multiplex expression profiling of both exogenous and endogenous transcripts from single cells allows for the immediate identification of TMs essential for direct cell reprogramming.

First, to ascertain accurate detection of exogenous genes, single cells expressing Venus fluorescent protein (i.e. 18-virus pool infected fibroblasts) were individually sorted using FACS and subjected to a multiplex Nesc-PCR for the detection of 18 virus-specific transcripts (Figure 1B). Based on our statistical analysis, the single-cell transduction followed the Poisson distribution and the number of detected genes correlated with the half of estimated number of virus particles per cell (Figure 1C). This suggests that a minimum of two copies of viral transcripts can be detected, and 10 MOI of the pooled virus, or 0.55 MOI per gene, was optimal to detect multiple target

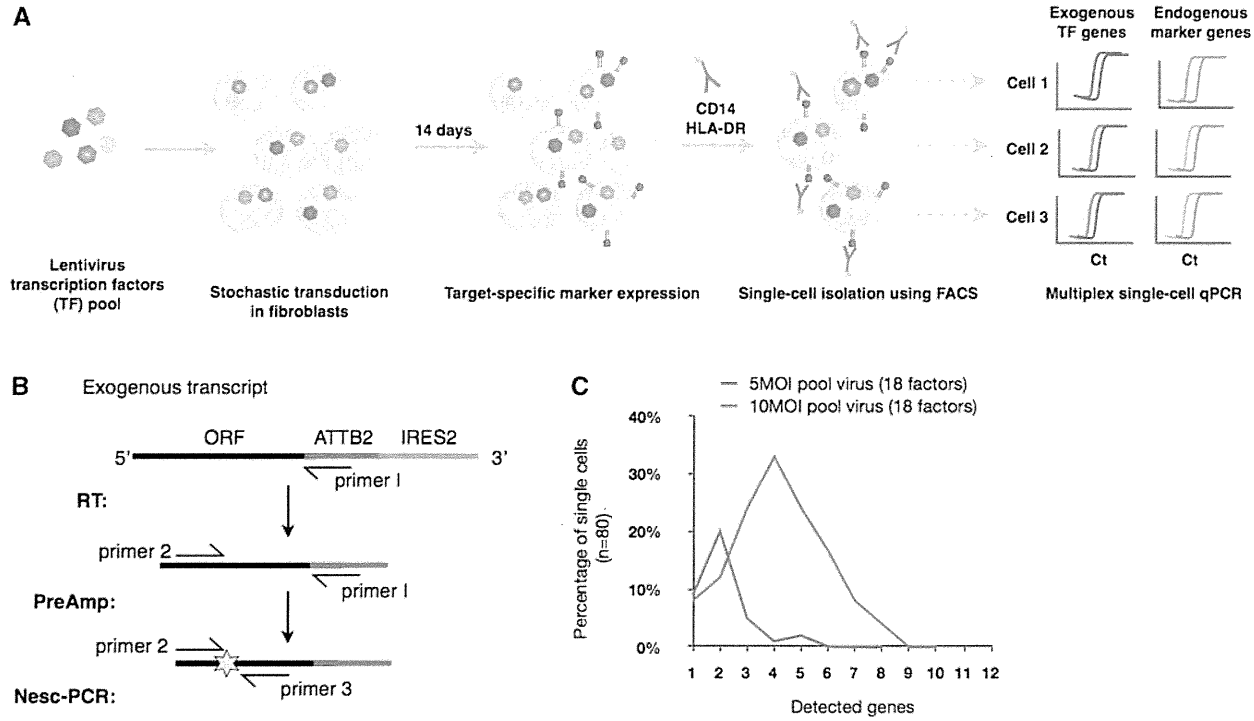

Figure 1. Workflow of single-cell screening and Nested-single-cell-PCR (Nesc-PCR). (**A**) Lentviruses encoding multiple transcription 'modulating' factors (TMs) are pooled and transduced into human dermal fibroblasts for a period of 2 weeks. Because of the stochastic nature of virus infection, a variety of TM combinations are expressed at random per single cell. Cells expressing a defined set of TMs give rise to the expression of target-cell-specific markers (e.g. CD14 and HLA-DR) allowing them to be individually sorted using FACS. Subsequently, single cells are profiled using a Nesc-PCR gene expression analysis by reverse transcribing (RT) the exogenous transcripts with a virus-specific primer (primer 1) followed by 18 cycles of pre-amplification with gene-specific forward primers (primer 2) and primer 1. The cDNA products are then subjected to a microfluidic qPCR for the identification of exogenous transcripts using gene-specific sense (primer 2) and anti-sense (primer 3) primer pairs and fluorescence probes (yellow star) (**B**). (**C**) The single cells transduced with pooled lentivirus (18 factors) at 5 MOI and 10 MOI were sorted and profiled using Nesc-PCR. At 10 MOI, >30% of single cells expressed 4 out of 18 TMs, while 20% of single cells expressed 2 out 18 TMs at 5 MOI.

genes from single cells since >50% of the population contained average number of two to six genes.

Single-cell gene expression analysis of virus-infected fibroblasts

CD14 and HLA-DR proteins have been well characterized to play a role in LPS response and antigen presentation in monocytes, respectively (24,25). To determine which of the 18 factors were critical for activating monocyte gene expression, we labeled the transduced cells using CD14 and HLA-DR antibodies. Two weeks post-infection at 10 MOI, 18 ± 2% of the fibroblasts showed Venus fluorescence (Figure 2A). Predictably from a pooled virus, a minute amount of Venus$^+$ cells were positive for both CD14 and HLA-DR (0.17 ± 0.1%; Figure 2B) but was sufficient to obtain single cells for transcript profiling using Nesc-PCR (M+, n = 86). To analyze the enrichment of TMs in marker-positive single cells, we additionally sorted an equal number of single cells from Venus$^+$ population as a baseline control (Figure 2A, M−). Additionally, fibroblasts transduced with vector control (10 MOI) failed to express CD14 and HLA-DR surface markers (data not shown).

Individually sorted single cells were profiled specifically targeting 18 viral-TM genes, 16 endogenous monocyte markers and 1 internal control (Supplementary Table S2). The final 35 monocyte–gene panel was used to measure by means of Nesc-PCR. To further address the effect of exogenous factors on fibroblasts, we additionally isolated and analyzed single cells from 'unperturbed' fibroblasts and human CD14$^+$ primary monocytes (n = 40 each, Supplementary Figure S2A). These individual cells were profiled using the same 35-gene panel but targeting 18 endogenous TMs.

We then analyzed the ability of Nesc-PCR gene expression analysis to distinguish different cell populations based on exogenous TMs and endogenous marker expressions. Figure 3A reveals a cluster of 86 CD14$^+$/HLA-DR$^+$ cells (M+) and 86 Venus$^+$ cells (M−). Most notably, single cells positive for CD14 and HLA-DR markers detected SPI1 (86/86, 100%) and 76 out of 86 expressed HCLS1 (88%), which were statistically significant when compared with the M− population where only 8/86 and 10/86 single cells were positive for SPI1 and HCLS1, respectively (chi-square test, P value < 0.001 for both). Interestingly, though eight out of nine single cells expressing exogenous SPI1 in the M− population expressed CD14 transcripts, and two out of nine expressed HLA-DRA transcripts, but no detection of HLA-DRB transcript was observed. Although the sample size was small, the analysis

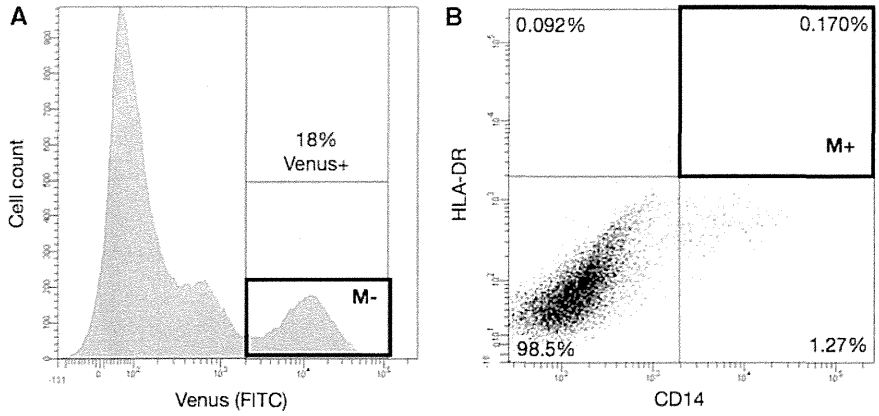

Figure 2. Flow cytometry sorting of CD14 and HLA-DR-positive single cells. Two weeks post transduction of 18 monocyte-TMs, 18% of fibroblasts expressed Venus fluorescent protein (A, 'M−'), out of which 0.17% was positive for both CD14 and HLA-DR markers (B, 'M+'). Eighty-six single cells from M+ and M−boxes were sorted for further analysis.

suggests that SPI1 alone could induce the expression of CD14. In fact, when SPI1 alone was transduced into fibroblasts in an independent experiment, 12 ± 2% of $SPI1^+$ cells expressed the CD14 surface marker suggesting that SPI1 could elicit the expression of this marker but at a low efficiency (Supplementary Figure S3).

In a drastic contrast to the M− population, the analysis of M+ population noticeably revealed that this subset, although transcriptionally heterogeneous, was almost exclusively composed of cells expressing high levels of genes characteristic of mature monocytes (Figure 3A). Single cells selected for CD14 and HLA-DR surface proteins revealed 100% detection of CD14, HLA-DRA and HLA-DRB marker transcripts, as expected. But additional markers such as CSF1R (85%), ILT4 (73%), TYROBP (63%) and CD163 (52%) transcripts were highly enriched in the M+ population when compared with the M− population (chi-square test, P value < 0.05) and significantly induced when compared with the basal expressions in dermal fibroblasts (Supplementary Figure S4).

SPI1 and HCLS1 as key determinants of monocyte expression

To further investigate the key regulatory determinants of monocyte specification, we performed eigenvector-based analyses between M+, M−, fibroblasts and monocytes to visualize the heterogeneity in single cells, as reflected by the 2-axis of the principal component analysis (PCA; Figure 3B). The analysis found that the first principal component (explaining 27.57% of the variation) grouped the primary monocytes and the M+ cells but separated fibroblasts and M− cells. These distinct clusters indicate that M+ cells deviated from the original fibroblast state and transitioned into a state comparable to that of $CD14^+$ monocytes. However, a closer examination of the second component narrowly distinguished the monocytes from the M+ cells, indicative of partial (or incomplete) induction of monocyte network in fibroblasts. The PCA also showed a wide scatter of M− single cells largely due to random virus transductions. However, a small number of single cells clustered closely to the M+ population largely contributed by positive detection of SPI1 and CD14 expression but failed to be selected by FACS due to lack of HLA-DR protein expression.

To identify the causal genes that contribute to the separation of each cell population, we performed the correspondence analysis (CoA; Figure 4C). Complementary to PCA, the CoA identified SPI1 and HCLS1 as major determinants to discriminate the monocytes from the original fibroblasts. Although the primary monocytes expressed SPI1 and HCLS1, the exogenous expression in the M+ population was 6-fold higher (in the case of SPI1), contributing to the separation from the primary monocytes on the second axis. Interestingly, the single-cell expression profile of primary monocytes revealed that 27% and 22% monocytes expressed CEBPA and IRF8, respectively, which is in contrast to the ubiquitous expression of SPI1 and HCLS1 in all 40 monocyte single cells profiled (Supplementary Figure S2B). The heterogeneous expressions of CEBPA and IRF8 transcripts may suggest a dynamic balance of expression to maintain monocyte phenotype but are not necessary required to promote key monocyte-specific markers.

SPI1 is required and HCLS1 enhances expression and function specific to monocytes

To further explore the effects of combinatorial TMs, we ectopically expressed vector control, SPI1, SPI1+HCLS1 in fibroblast and measured the differential expression using the conventional qRT-PCR method. CSF1R is a well-studied monocyte membrane protein acting as a receptor for colony stimulating factor 1, and deregulation of this gene is a hallmark of many tumors (26). Although SPI1 alone could induce the expression of this monocyte marker, the signal intensity was greatly enhanced when fibroblasts were co-infected with HCLS1 (Figure 4A). Similar expression patterns were also observed for TYROBP and CD163. However, HCLS1 could not enhance the transcript level of CD14. When the induced expressions were compared with the basal expression of monocytes, the cell transformation was only partial

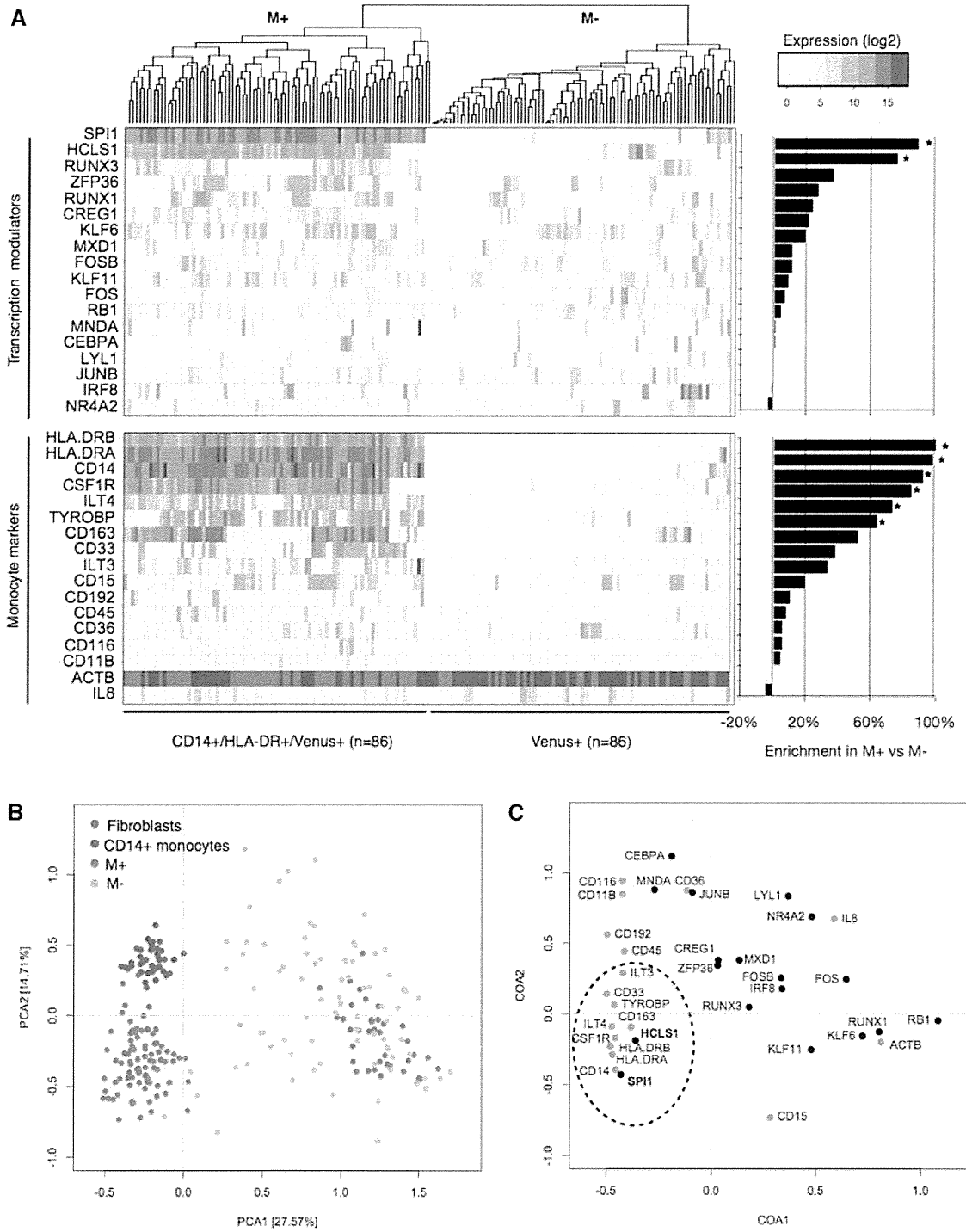

Figure 3. Single-cell clustering analyses. Hierarchical clustering of single cells reveals distinct cell populations between M+ and M− (**A**). The gene enrichment comparisons between M+ and M− population demonstrates differential detection rate of TMs as well as monocyte-marker transcripts. (**B**) The principal component analysis (PCA) demonstrates variations of single cells from four populations: $CD14^+$ primary monocytes, dermal fibroblasts, $CD14^+$/HLA-DR^+/$Venus^+$ (M+), $CD14^-$/HLA-DR^-/$Venus^+$ (M−). The M− population (orange) clusters near the fibroblasts (red) and shows the largest variation, mainly due to random detection of exogenous TMs. However, the M+ population (green) reveals reduced variation and clusters near the primary monocytes (blue). (**C**) The correspondence analysis reveals SPI1 and HCLS1 TMs (bolded; bottom-left) as key determinants of M+ population, causing the separation of M+ cells from fibroblasts and shifting the M+ cells towards monocytes. Gene enrichment analysis, chi-square test P value < 0.005.

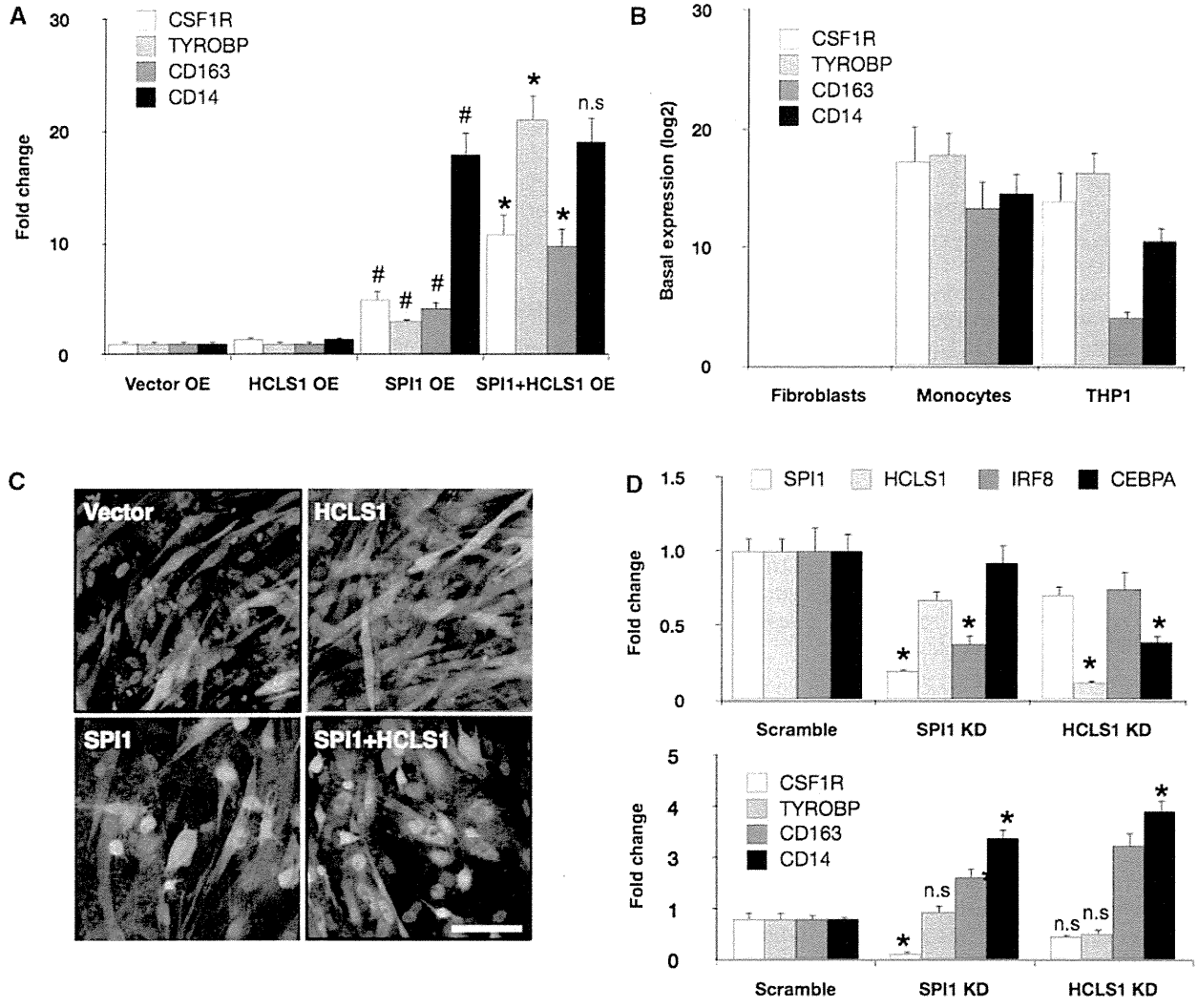

Figure 4. SPI1 and HCLS1 enhance monocyte marker expression and function. Vector control, HCLS1, SPI1 and SPI1/HCLS1 combination were overexpressed (OE) in dermal fibroblasts, and the marker expressions for CSF1R, TYROBP, CD163 and CD14 were quantified by means of conventional qRT-PCR expression analysis (**A**). (Student's *t*-test: #*P* value < 0.05 when compared with vector control; **P* value < 0.05 when compared with SPI1 or HCLS1 alone). However, the induced marker expressions were partial when compared with the basal expression levels (log-2 transformed) of dermal fibroblasts, primary monocytes and THP1 cell line (**B**). (**C**) pHrodo™ Red *E. coli* BioParticles® conjugate beads which is pH-sensitive Rhodamine dye specifically expressed in phagosomes were added onto fibroblasts transduced with either vector control, SPI1, HCLS1 or SPI1/HCLS1. Cells positive for Rhodamine (red) were clearly visible in both SPI1 and SPI1/HCLS1 combination, but no detection was found in cells transduced only with vector control or HCLS1. Scale bar = 100 μm. (**D**) Gene-specific knockdown (KD) of SPI1 and HCLS1 in THP1 cells revealed significant suppression of IRF8 and CEBPA transcripts, respectively. Knockdown of SPI1 also suppressed CSF1R, but induced CD163 and CD14 expression, which was also observed when HCLS1 transcript was ablated. *P* value (Student's *t*-test) * < 0.001, when compared with vector control.

(Figure 4B). This incomplete observation was also seen in the single-cell PCA analysis (Figure 3B), indicating that the conversion is heterogeneous and partial, although some single cells clustered closer to the primary monocytes than others. Concurrently, it is also plausible that only a subpopulation of the cells undergoes cell transformation, diluting the expression levels and thus masking the induced expression.

Next to test whether SPI1 in conjunction with HCLS1 could also enhance the functional role of monocytes, we added pHrodo™ Red *E. coli* BioParticles® conjugate beads, which is pH-sensitive Rhodamine dye to fibroblasts transduced with lentivirus vector control, SPI1, HCLS1 or both (Figure 4C; Supplementary Figure S5). Since the fluorescent dye of the beads specifically expresses in phagosomes, we could reliably detect the ingested beads using the fluorescent microscopy without trypsinization of the cells. We observed a clear detection of Rhodamine-positive cells after transducing SPI1 and the SPI1/HCLS1 combination. The image analysis further revealed that cells transduced in combination of SPI1 and HCLS1 ingested 33% more beads when compared with SPI1 alone (Supplementary Figure S5B).

To better understand the causal effects of SPI1 and HCSL1 involved in monocyte specification, we targeted the transcripts using siRNA oligos in THP1 (human

acute monocytic leukemia cell line). THP1 has been reported to be a suitable model to study monocyte network (16) and also has been demonstrated to yield high efficiencies in siRNA transfections (16,27). Since IRF8 and CEBPA have been implicated as key regulators of monocyte network, we specifically measured the expression changes after the knockdown (16,18,28,29). Interestingly, ablating SPI1 and HCLS1 transcripts in THP1 cells could significantly repress IRF8 and CEBPA expression by 2.71-fold and 2.56-fold, respectively (Figure 4D), as well as CSF1R by 6.41-fold—in the case of SPI1 (Figure 4E). Surprisingly, however, THP1 deficient in SPI1 augmented CD163 and CD14 expression, and a similar expression pattern was also observed for the HCLS1 knockdown. Although the exact mechanisms is unclear, ablation of SPI1 and/or HCLS1 in the established monocyte network may not be sufficient to suppress marker genes such as TYROBP ('gene redundancy') or may induce gene expressions to maintain network homeostasis ('network robustness'). Taken together, our results revealed that SPI1 is minimally required to promote, in part, monocytic expression and phagocytic function in human dermal fibroblasts but can be greatly enhanced through the co-expression of HCLS1.

DISCUSSION

Here we described a rapid and direct method that facilitates the use of lentivirus and Nesc-PCR for identifying key genes involved in trans-differentiation. By relying on the random nature of virus infection, we implemented a single-cell 'shotgun-transduction' system that enabled the prompt detection, isolation and identification of combinatorial genes that are required to transform fibroblasts into a desired target cell type.

By taking advantage of viral transcripts and the single-cell detection method, we noted SPI1 and HCLS1 as a defined set of transcription modulators responsible to switch from human dermal fibroblasts to functional monocyte-like cells. SPI1, an important regulator of myeloid and B-lymphoid cell development, also acts as a key modulator of cell transformation toward monocytes together with CEBPA (9). The detection of SPI1 by the single-cell screening system decisively validates our method in identifying the strongest modulator in the group. However, we could additionally demonstrate that CEBPA was dispensable in that SPI1 alone could induce the expression of CD14 and HLA-DRA and promote phagocytosis in human fibroblasts. Although HCLS1 alone could not induce monocyte trans-differentiation, the protein acted as a strong modulator of monocyte/macrophage phenotype. HCLS1 has been implicated in response to cortisol and LPS, activating numerous functions of macrophages (30,31). Although the exact mechanism is unknown, our data and the published reports strongly suggest that HCLS1 expression correlates positively with enhanced function of monocytes/macrophages possibly via regulating CEBPA expression.

In this study, we have validated a highly scalable approach for screening lentiviral libraries for direct cell reprogramming. We used cell-specific markers to isolate single cells; however, this method can virtually be applied to any characteristics that allow separation of phenotypically distinct cells, such as cell proliferation dyes or functional biomarkers for the identification of transcription modulators. Overall, this study demonstrates a rapid single-cell screening workflow to readily identify and characterize new combinatorial factors, applicable to induce various cell-reprogramming pathways.

SUPPLEMENTARY DATA

Supplementary Data are available at NAR Online: Supplementary Tables 1 and 2 and Supplementary Figures 1–5.

ACKNOWLEDGEMENTS

We thank members of Omics Science Center (RIKEN Yokohama) for virus production (Chiduru Suzuki, Ayumi Ogawa, Yumi Yoshimura and Akane Murakami), cloning/sequence verification (GeNas) and statistical analysis (Michiel De Hoon). We also extend our gratitude to Dr. Hiroyuki Miyoshi (RIKEN BRC) for providing the lentivirus vectors and Drs. Osamu Ohara and Yoshitaka Shirasaki (RIKEN RCAI) for the use of the Fluidigm Biomark system.

FUNDING

Research fund for Foreign Postdoctoral Researcher Program from RIKEN (to J.W.S.); Research Grant for RIKEN Omics Science Center from MEXT (to Y. Hayashizaki); Grant of the Innovative Cell Biology by Innovative Technology (Cell Innovation Program) from the MEXT (to Y. Hayashizaki) and Strategic programs for R&D (Presidents discretionary fund) (super immune cell) (to Y. Hayashizaki). Funding for open access charge: Research Grant for RIKEN Omics Science Center from MEXT (to Y. Hayashizaki).

Conflict of interest statement. None declared.

REFERENCES

1. Ieda,M., Fu,J.D., Delgado-Olguin,P., Vedantham,V., Hayashi,Y., Bruneau,B.G. and Srivastava,D. (2010) Direct reprogramming of fibroblasts into functional cardiomyocytes by defined factors. *Cell*, **142**, 375–386.
2. Takahashi,K., Tanabe,K., Ohnuki,M., Narita,M., Ichisaka,T., Tomoda,K. and Yamanaka,S. (2007) Induction of pluripotent stem cells from adult human fibroblasts by defined factors. *Cell*, **131**, 861–872.
3. Yu,J., Vodyanik,M.A., Smuga-Otto,K., Antosiewicz-Bourget,J., Frane,J.L., Tian,S., Nie,J., Jonsdottir,G.A., Ruotti,V., Stewart,R. *et al.* (2007) Induced pluripotent stem cell lines derived from human somatic cells. *Science*, **318**, 1917–1920.
4. Stadtfeld,M., Maherali,N., Breault,D.T. and Hochedlinger,K. (2008) Defining molecular cornerstones during fibroblast to iPS cell reprogramming in mouse. *Cell Stem Cell*, **2**, 230–240.
5. Bai,Y., Soda,Y., Izawa,K., Tanabe,T., Kang,X., Tojo,A., Hoshino,H., Miyoshi,H., Asano,S. and Tani,K. (2003) Effective transduction and stable transgene expression in human blood cells by a third-generation lentiviral vector. *Gene Ther.*, **10**, 1446–1457.

6. Miyoshi,H., Blomer,U., Takahashi,M., Gage,F.H. and Verma,I.M. (1998) Development of a self-inactivating lentivirus vector. *J. Virol.*, **72**, 8150–8157.
7. Takahashi,K. and Yamanaka,S. (2006) Induction of pluripotent stem cells from mouse embryonic and adult fibroblast cultures by defined factors. *Cell*, **126**, 663–676.
8. Zhou,Q., Brown,J., Kanarek,A., Rajagopal,J. and Melton,D.A. (2008) In vivo reprogramming of adult pancreatic exocrine cells to beta-cells. *Nature*, **455**, 627–632.
9. Feng,R., Desbordes,S.C., Xie,H., Tillo,E.S., Pixley,F., Stanley,E.R. and Graf,T. (2008) PU.1 and C/EBPalpha/beta convert fibroblasts into macrophage-like cells. *Proc. Natl Acad. Sci. USA*, **105**, 6057–6062.
10. Vierbuchen,T., Ostermeier,A., Pang,Z.P., Kokubu,Y., Sudhof,T.C. and Wernig,M. (2010) Direct conversion of fibroblasts to functional neurons by defined factors. *Nature*, **463**, 1035–1041.
11. Sekiya,S. and Suzuki,A. (2011) Direct conversion of mouse fibroblasts to hepatocyte-like cells by defined factors. *Nature*, **475**, 390–393.
12. Maherali,N., Sridharan,R., Xie,W., Utikal,J., Eminli,S., Arnold,K., Stadtfeld,M., Yachechko,R., Tchieu,J., Jaenisch,R. *et al.* (2007) Directly reprogrammed fibroblasts show global epigenetic remodeling and widespread tissue contribution. *Cell Stem Cell*, **1**, 55–70.
13. Papapetrou,E.P., Lee,G., Malani,N., Setty,M., Riviere,I., Tirunagari,L.M., Kadota,K., Roth,S.L., Giardina,P., Viale,A. *et al.* (2011) Genomic safe harbors permit high beta-globin transgene expression in thalassemia induced pluripotent stem cells. *Nat. Biotechnol.*, **29**, 73–78.
14. Singh,S.K., Clarke,I.D., Terasaki,M., Bonn,V.E., Hawkins,C., Squire,J. and Dirks,P.B. (2003) Identification of a cancer stem cell in human brain tumors. *Cancer Res.*, **63**, 5821–5828.
15. Vuk-Pavlovic,S., Bulur,P.A., Lin,Y., Qin,R., Szumlanski,C.L., Zhao,X. and Dietz,A.B. (2010) Immunosuppressive CD14+HLA-DRlow/- monocytes in prostate cancer. *Prostate*, **70**, 443–455.
16. Suzuki,H., Forrest,A.R., van Nimwegen,E., Daub,C.O., Balwierz,P.J., Irvine,K.M., Lassmann,T., Ravasi,T., Hasegawa,Y., de Hoon,M.J. *et al.* (2009) The transcriptional network that controls growth arrest and differentiation in a human myeloid leukemia cell line. *Nat. Genet.*, **41**, 553–562.
17. Ravasi,T., Suzuki,H., Cannistraci,C.V., Katayama,S., Bajic,V.B., Tan,K., Akalin,A., Schmeier,S., Kanamori-Katayama,M., Bertin,N. *et al.* (2010) An atlas of combinatorial transcriptional regulation in mouse and man. *Cell*, **140**, 744–752.
18. Suzuki,T., Nakano-Ikegaya,M., Yabukami-Okuda,H., de Hoon,M., Severin,J., Saga-Hatano,S., Shin,J.W., Kubosaki,A., Simon,C., Hasegawa,Y. *et al.* (2012) Reconstruction of monocyte transcriptional regulatory network accompanies monocytic functions in human fibroblasts. *PloS One*, **7**, e33474.
19. Ashburner,M., Ball,C.A., Blake,J.A., Botstein,D., Butler,H., Cherry,J.M., Davis,A.P., Dolinski,K., Dwight,S.S., Eppig,J.T. *et al.* (2000) Gene ontology: tool for the unification of biology. The Gene Ontology Consortium. *Nat. Genet.*, **25**, 25–29.
20. Gentleman,R.C., Carey,V.J., Bates,D.M., Bolstad,B., Dettling,M., Dudoit,S., Ellis,B., Gautier,L., Ge,Y., Gentry,J. *et al.* (2004) Bioconductor: open software development for computational biology and bioinformatics. *Genome Biol.*, **5**, R80.
21. Schutze,K. and Lahr,G. (1998) Identification of expressed genes by laser-mediated manipulation of single cells. *Nat. Biotechnol.*, **16**, 737–742.
22. Tiller,T., Meffre,E., Yurasov,S., Tsuiji,M., Nussenzweig,M.C. and Wardemann,H. (2008) Efficient generation of monoclonal antibodies from single human B cells by single cell RT-PCR and expression vector cloning. *J. Immunol. Methods*, **329**, 112–124.
23. Marcus,J.S., Anderson,W.F. and Quake,S.R. (2006) Microfluidic single-cell mRNA isolation and analysis. *Anal. Chem.*, **78**, 3084–3089.
24. Hershman,M.J., Cheadle,W.G., Wellhausen,S.R., Davidson,P.F. and Polk,H.C. Jr (1990) Monocyte HLA-DR antigen expression characterizes clinical outcome in the trauma patient. *Brit. J. Surg.*, **77**, 204–207.
25. Kirschning,C.J., Wesche,H., Merrill Ayres,T. and Rothe,M. (1998) Human toll-like receptor 2 confers responsiveness to bacterial lipopolysaccharide. *J. Exp. Med.*, **188**, 2091–2097.
26. Bonifer,C. and Hume,D.A. (2008) The transcriptional regulation of the Colony-Stimulating Factor 1 Receptor (csf1r) gene during hematopoiesis. *Front Biosci.*, **13**, 549–560.
27. Tomaru,Y., Simon,C., Forrest,A.R., Miura,H., Kubosaki,A., Hayashizaki,Y. and Suzuki,M. (2009) Regulatory interdependence of myeloid transcription factors revealed by Matrix RNAi analysis. *Genome Biol.*, **10**, R121.
28. Kubosaki,A., Lindgren,G., Tagami,M., Simon,C., Tomaru,Y., Miura,H., Suzuki,T., Arner,E., Forrest,A.R., Irvine,K.M. *et al.* (2010) The combination of gene perturbation assay and ChIP-chip reveals functional direct target genes for IRF8 in THP-1 cells. *Mol. Immunol.*, **47**, 2295–2302.
29. Geissmann,F., Manz,M.G., Jung,S., Sieweke,M.H., Merad,M. and Ley,K. (2010) Development of monocytes, macrophages, and dendritic cells. *Science*, **327**, 656–661.
30. Rodriguez,N., Mages,J., Dietrich,H., Wantia,N., Wagner,H., Lang,R. and Miethke,T. (2007) MyD88-dependent changes in the pulmonary transcriptome after infection with Chlamydia pneumoniae. *Physiol. Genomics*, **30**, 134–145.
31. Billing,A.M., Fack,F., Turner,J.D. and Muller,C.P. (2011) Cortisol is a potent modulator of lipopolysaccharide-induced interferon signaling in macrophages. *Innate Immun.*, **17**, 302–320.

Neurochemistry International 61 (2012) 240–250

Contents lists available at SciVerse ScienceDirect

Neurochemistry International

journal homepage: www.elsevier.com/locate/nci

Linkage of N-cadherin to multiple cytoskeletal elements revealed by a proteomic approach in hippocampal neurons

Hidekazu Tanaka [a,*], Kazuaki Takafuji [a], Akihiko Taguchi [b], Pattama Wiriyasermkul [a], Ryuichi Ohgaki [a], Shushi Nagamori [a], Pann-Ghill Suh [c], Yoshikatsu Kanai [a]

[a] Department of Pharmacology, Osaka University School of Medicine, Osaka 565-0871, Japan
[b] Institute of Biomedical Research and Innovation, Kobe 650-0047, Japan
[c] Advanced Research Center for Signal Transduction in Cancers, Ulsan National Institute of Science and Technology, Ulsan 689-798, Republic of Korea

ARTICLE INFO

Article history:
Received 5 April 2012
Received in revised form 7 May 2012
Accepted 9 May 2012
Available online 17 May 2012

Keywords:
Synapse
Plasticity
Adhesion
Cadherin
Cytoskeleton
Hippocampus

ABSTRACT

The CNS synapse is an adhesive junction differentiated for chemical neurotransmission and is equipped with presynaptic vesicles and postsynaptic neurotransmitter receptors. Cell adhesion molecule cadherins not only maintain connections between pre- and postsynaptic membranes but also modulate the efficacy of synaptic transmission. Although the components of the cadherin-mediated adhesive apparatus have been studied extensively in various cell systems, the complete picture of these components, particularly at the synaptic junction, remains elusive. Here, we describe the proteomic assortment of the N-cadherin-mediated synaptic adhesion apparatus in cultured hippocampal neurons. N-cadherin immunoprecipitated from Triton X-100-solubilized neuronal extract contained equal amounts of β- and α-catenins, as well as F-actin-related membrane anchor proteins such as integrins bridged with α-actinin-4, and Na^+/K^+-ATPase bridged with spectrins. A close relative of β-catenin, plakoglobin, and its binding partner, desmoplakin, were also found, suggesting that a subset of the N-cadherin-mediated adhesive apparatus also anchors intermediate filaments. Moreover, dynein heavy chain and LEK1/CENPF/mitosin were found. This suggests that internalized pools of N-cadherin in trafficking vesicles are conveyed by dynein motors on microtubules. In addition, ARVCF and NPRAP/neurojungin/δ2-catenin, but not p120ctn/δ1-catenin or plakophilins-1, -2, -3, -4 (p0071), were found, suggesting other possible bridges to microtubules. Finally, synaptic stimulation by membrane depolarization resulted in an increased 93-kDa band, which corresponded to proteolytically truncated β-catenin. The integration of three different classes of cytoskeletal systems found in the synaptic N-cadherin complex may imply a dynamic switching of adhesive scaffolds in response to synaptic activity.

1. Introduction

The CNS synapse is an adhesive junction differentiated for chemical transmission and is equipped with presynaptic vesicles and postsynaptic neurotransmitter receptors. Cell adhesion molecules that link pre- and postsynaptic membranes not only maintain specific synaptic connections but also regulate the efficacy of synaptic transmission and plasticity (Bozdagi et al., 2004; Jungling et al., 2006; Okamura et al., 2004; Tanaka et al., 2000). Proteins assembled for the cadherin-mediated adherens junction have been extensively studied in various cell systems. However, different cadherins have been studied in distinct cell system models. Hence, it is unclear which proteins are genuinely assembled in synaptic junctions.

Cadherins are large superfamily of transmembrane cell adhesion proteins with characteristic extracellular repeats of about 110 amino acids. The cadherin superfamily comprises the classic cadherin and protocadherin subfamilies. Classic cadherins share conserved cytoplasmic domains that bind to β-catenin, whereas protocadherins have diversiform cytoplasmic domains connected to a wide variety of intracellular signaling molecules (Yagi and Takeichi, 2000). Classic cadherins are expressed in synaptic junctions (Benson and Tanaka, 1998; Fannon and Colman, 1996; Manabe et al., 2000; Uchida et al., 1996). Among them, N-cadherin

Abbreviations: AMPA, 2-amino-3-(5-methyl-3-oxo-1,2-oxazol-4-yl)propanoic acid; CNS, central nervous system; HBSS, Hanks' balanced salt solution; LC–MS/MS, liquid chromatography–tandem mass spectrometry; MAP kinase, mitogen-activated protein kinase; MT, microtubule; NMDA, *N*-methyl-D-aspartate; PAGE, polyacrylamide gel electrophoresis; PPW, presynaptic particle web; PSD, postsynaptic density; SDS, sodium dodecyl sulfate.

* Corresponding author. Address: Department of Pharmacology A6, Osaka University School of Medicine, 2-2 Yamadaoka, Suita, Osaka 565-0871, Japan. Tel.: +81 6 6879 3521; fax: +81 6 6879 3529.
E-mail address: htanaka@pharma1.med.osaka-u.ac.jp (H. Tanaka).

0197-0186/$ - see front matter © 2012 Elsevier Ltd. All rights reserved.
http://dx.doi.org/10.1016/j.neuint.2012.05.008

has been intensively investigated in hippocampal neurons and has been proven to play various roles in synaptic transmission and plasticity (Bozdagi et al., 2000; Jungling et al., 2006; Tang et al., 1998). The involvement of N-cadherin in synaptic activity is also supported by studies on cadherin-interacting proteins such as β-catenin (Okuda et al., 2007), δ-catenin (Israely et al., 2004), and IQ-GAP/ERK (Schrick et al., 2007).

Accumulating evidence indicates the involvement of N-cadherin as a dynamic feature of synaptic physiology. For example, N-cadherin mediates an activity-induced enlargement of the dendritic spine, which is dependent on rearrangement of the actin cytoskeleton (Okamura et al., 2004). Concomitantly, N-cadherin can undergo conformational change, e.g. dimerization, with acquired resistance to trypsin (Tanaka et al., 2000). At the same time, N-cadherin shows enhanced binding to β-catenin (Murase et al., 2002) and stabilization on the cell surface (Tai et al., 2007). The immobilization of N-cadherin/β-catenin parallels with the stabilization of actin filaments by synaptic stimulation (Fischer et al., 2000; Fukazawa et al., 2003; Lin et al., 2005; Okamoto et al., 2004; Star et al., 2002). There are also suggestions that the N-cadherin–catenin complex is more directly linked to presynaptic vesicular physiology (Bamji et al., 2003, 2006; Bozdagi et al., 2004; Jungling et al., 2006) as well as postsynaptic neurotransmitter receptors (Saglietti et al., 2007). Furthermore, there are pathways that force N-cadherin into intracellular compartments. One pathway involves steady-state endocytosis, which is inhibited by the activation of the NMDA receptor (Tai et al., 2007). Another is an activity-regulated endocytic pathway, in which arcadlin (protocadherin-8), induces endocytosis of N-cadherin as a downstream event of p38 MAP kinase activation (Yasuda et al., 2007).

Thus, N-cadherin plays multiple, dynamic roles in synaptic remodeling and plasticity. Synaptic N-cadherin should therefore be linked to distinct cellular mechanisms that are specialized for separate, specific tasks. Here, we focus on the rodent hippocampal synapse to directly depict the cadherin-mediated adhesion complex. We describe the proteomic assortment of the synaptic adhesion apparatus assisted by N-cadherin in cultured hippocampal neurons. The protein complexes assembled with N-cadherin were consistent with the N-cadherin linkages to F-actins, intermediate filaments, and microtubules. In addition, synaptic stimulation by membrane depolarization resulted in the increase of a 93-kDa band, which corresponded to proteolytically truncated β-catenin. The integration of three different cytoskeletal systems takes place in N-cadherin-mediated adhesive machinery, providing a dynamic scaffold underlying synaptic plasticity.

2. Materials and methods

2.1. Neuron culture

Hippocampal neurons were cultured from E18 rat embryos as previously described (Tanaka et al., 2000). Neurons were plated at a density of 1.4–2.1 × 10^4 cells/cm^2 onto poly-L-lysine-coated dishes (Φ = 35 mm). Neurons were maintained in Neurobasal medium supplemented with B27 (Life Technologies) and 5 μM cytosine arabinoside.

2.2. Protein extraction, immunoprecipitation, and immunoblotting

Hippocampi were dissected from adult C57BL/6 mice, homogenized in Ca-PI-lysis buffer (10 mM HEPES–NaOH (pH 7.4), 1% Triton X-100, 120 mM NaCl, 2 mM $CaCl_2$, 10 μg/ml leupeptin, 10 μg/ml pepstatin A, 1 μg/ml aprotinin, 0.2 mM phenylmethylsulfonyl fluoride, 20 mM NaF, 20 mM β-glycerophosphate, and 1 mM Na_3VO_4) with a Teflon-glass homogenizer, and centrifuged for 1 h to obtain clear protein extracts. Mature neurons cultured for 4–5 weeks were depolarized with 50 mM KCl for 15 min. Neurons were washed twice with chilled PBS, harvested with 80 μl (for a Φ = 35 mm dish) of Ca-PI-lysis buffer, sonicated, and centrifuged. N-cadherin-associated protein complex was immunoprecipitated from these samples with 0.5–2.5 μg of murine anti-N-cadherin (BD Transduction Laboratories). The precipitated protein complex was separated in 4–15% gradient SDS–PAGE followed by either silver staining, Sypro Ruby (Molecular Probes) staining, or immunoblotting. Immunoblots were probed with murine anti-α-catenin (BD Transduction Laboratories, 1:5000), murine anti-p120 (BD Transduction Laboratories, 1:2500), murine anti-plakoglobin (BD Transduction Laboratories, 1:2000), rabbit anti-syntaxin 1 (Sigma–Aldrich, 1:10000), rabbit anti-JLP (SPAG9) (Abcam, 1:10000), rabbit anti-pan-14-3-3 (Millipore, 1:5000), murine anti-TRAP1 (BD Transduction Laboratories 1:5000), rabbit anti-DDB1 (Abcam, 1:5000), and rabbit anti-TRIM33 (Bethyl Laboratories, 1:2000) antibodies.

2.3. Sequential extraction of synaptosome fractions

Hippocampi isolated from two mice were homogenized (Dounce homogenizer, 30 strokes) in buffered sucrose (0.32 M sucrose in hypotonic A buffer). Hypotonic A buffer contained 4 mM HEPES–NaOH (pH 7.4), 1 mM $MgCl_2$, 0.5 mM $CaCl_2$, and 0.0025% butylated hydroxy toluene. The homogenate was centrifuged (800g × 10 min) and the supernatant (S1) was centrifuged again (9200g × 15 min) to collect the precipitate (P2). The P2 pellet was resuspended in buffered sucrose and overlaid on stepwise sucrose gradients (0.85, 1.0, and 1.2 M) and ultracentrifuged at 82,500g for 120 min. The crude synaptosome fraction accumulated between 1.0 and 1.2 M cushions was collected, diluted with 3 × volume of hypotonic A buffer, and ultracentrifuged (32,800g × 20 min). The resultant synaptosome pellet was resuspended in 120 μl of isotonic buffer B (10 mM HEPES–NaOH (pH 7.4), 120 mM NaCl, 1 mM $MgCl_2$, 0.5 mM $CaCl_2$, 0.0025% butylated hydroxy toluene, 10 μg/ml leupeptin, 10 μg/ml pepstatin A, 1 μg/ml aprotinin, and 0.2 mM phenylmethylsulfonyl fluoride), mixed with 30 μl of 0.1 M methyl-β-cyclodextrin, and incubated at 37 °C for 15 min followed by centrifugation (15,000 rpm × 15 min at 23 °C). After removing the supernatant as a methyl-β-cyclodextrin extract, the pellet was resuspended in 150 μl of stripping buffer (5 M urea dissolved in isotonic buffer B) and centrifuged as previously to obtain a urea extract and stripped-membrane pellet. The urea-stripped membrane pellet was resuspended in 150 μl of solubilizing buffer (1% Triton X-100 dissolved in isotonic buffer B) and centrifuged to obtain a Triton extract and an insoluble pellet.

2.4. In-gel digestion

Gel pieces were excised from Sypro Ruby-stained gels and washed with 50% (v/v) acetonitrile and 50 mM NH_4HCO_3, pH 8.0, for 30 min to remove the fluorescence dye. Gel pieces were then soaked in acetonitrile for 5 min, acetonitrile was removed, and the gel pieces were dried for 20 min in a vacuum. Prior to enzymatic digestion, gel pieces were reduced with 10 mM dithiothreitol in 50 mM NH_4HCO_3 at 37 °C for 30 min, then alkylated with 55 mM iodoacetamide in 50 mM NH_4HCO_3 for 30 min, and dehydrated by addition of acetonitrile. The reduced and alkylated gel pieces were rehydrated in 50 mM Tris–HCl, pH 9.0, and 0.5 μg/ml sequencing grade modified trypsin (Roche Diagnostics). Once this solution was fully absorbed by the gel pieces, enzyme-free Tris–HCl buffer was added until the gel pieces were covered. The samples were digested for 16 h at 37 °C, extracted with acetonitrile and 5% formic acid for 20 min, and acetonitrile was evaporated using a Speed-Vac centrifuge. The tryptic digests were desalted

with C18-StageTips, concentrated using the Speed-Vac centrifuge, and reconstituted in 0.1% formic acid and 3% acetonitrile.

2.5. In-solution digestion for shotgun analyses

Immunoprecipitated samples were added to 50 mM Tris–HCl, pH 9.0, reduced with 10 mM dithiothreitol at 37 °C for 30 min, alkylated with 55 mM iodoacetamide in the dark at room temperature for 30 min, and digested with 0.5 μg/ml sequencing grade modified trypsin at 37 °C for 16 h. The digests were desalted and reconstituted as above.

2.6. LC–MS/MS and data analysis

LC–MS/MS analysis was performed by a Paradigm MS4 nano-HPLC system (Michrom BioResources, Inc., Auburn, CA) coupled to an LTQ linear ion trap mass spectrometer (Thermo Electron Corp., Waltham, MA) with a nanoelectrospray ionization source (AMR Inc., Tokyo, Japan). Tryptic peptides were injected by an HTC-PAL autosampler (CTC Analytics AG, Zwingen, Switzerland) and enriched on a C18 trap column (300 μm I.D. × 5 mm length, CERI, Tokyo, Japan) at a flow rate of 6 μl/min. The samples were subsequently separated by a C18 reverse phase column (100 μm I.D. × 150 mm length, Nikkyo Technos Co., Ltd., Tokyo, Japan) at a flow rate of 1 μl/min with a linear gradient from 2% to 65% mobile phase B, i.e. from 98% to 35% of mobile phase A. Mobile phase B consisted of 95% acetonitrile with 0.1% formic acid, whereas mobile phase A consisted of 2% acetonitrile with 0.1% formic acid. LC–MS/MS analysis was carried out using data-dependent triple-play mode. Automated gain control values were set at 1.5×10^4, 1.5×10^3, and 5.0×10^3 for Full-MS, Zoom-MS, and MS/MS, respectively. A spray voltage of 1.6 kV was applied. The MS scan range was *m/z* 300–2000. Peptides and proteins were identified by Mascot v2.2 (Matrix Science, London, UK) with a maximum tolerance of 1.2 Da for MS data, 0.5 Da for MS/MS data, and strict trypsin specificity allowing for up to one missed cleavage. Carbamidomethylation of cysteine and oxidation of methionine were allowed as a variable modification.

2.7. Trypsin treatment of living neurons

Modification of N-cadherin in response to synaptic stimulation was demonstrated by the acquired resistance to trypsin as reported (Tanaka et al., 2000). Stimulated and control neurons, maintained in 35 mm dishes (14,400 cells/cm^2), were washed briefly with prewarmed (37 °C) HEPES-buffered (10 mM, pH 7.4) HBSS and covered with 0.1% trypsin (Life Technologies) diluted with HBSS. The excess trypsin solution was removed immediately, followed by incubation for 10 min at 37 °C. The digested neurons were directly harvested in SDS–PAGE sample buffer (80 μl), or 40 μl of Ca-lysis buffer supplemented with soybean trypsin inhibitor (10 mM HEPES–NaOH (pH 7.4), 1% Triton X-100, 120 mM NaCl, 2 mM $CaCl_2$, 10 μg/ml leupeptin, 10 μg/ml pepstatin A, 1 μg/ml aprotinin, 0.2 mM phenylmethylsulfonyl fluoride, and 0.01% trypsin inhibitor) followed by centrifugation (15,000 rpm × 5 min at 4 °C) to obtain the Triton-soluble supernatant and the Triton-insoluble pellet. The supernatant was mixed with 5 × SDS–PAGE sample buffer (10 μl), and the pellet was resuspended in SDS–PAGE sample buffer containing 4 M urea (40 μl).

3. Results and discussion

3.1. Strategy

N-cadherin is expressed in synaptic membranes of hippocampal neurons (Benson and Tanaka, 1998; Tanaka et al., 2000). Synaptic N-cadherin appears to comprise: a surface pool in the endocytic zone located in the periphery of the synapse (Tanaka et al., 2000; Uchida et al., 1996), an intracellular pool such as endosomes (Tai et al., 2007; Yasuda et al., 2007), and an active zone pool associated with the presynaptic particle web (PPW) and postsynaptic density (PSD) (Fig. 1A) (Phillips et al., 2001).

The active zone-associated electron-dense structures (PPW + PSD), which correspond to so-called synaptic junctions, are biochemically characterized by the insolubility in 1% Triton X-100 (Phillips et al., 2001). Approximately 60% of N-cadherin was collected in the Triton-soluble fraction and 40% in the Triton-insoluble fraction (Fig. 1B,C). In the epithelial cells, the Triton-insoluble fraction is comprised of cytoskeleton-associated scaffolding protein complexes and cholesterol-rich lipid rafts (Brown and Rose, 1992). N-cadherin was not extracted from the crude synaptosome fraction with methyl-β-cyclodextrin, a cholesterol-extracting agent, suggesting that the Triton-insoluble N-cadherin is largely integrated into the synaptic junctional complex (Fig. 1B,C). Usually, biochemical analyses of the synaptic junctions utilize these Triton-insoluble PSD fractions (Cotman et al., 1974). For example, in immunoprecipitation experiments, the PSD is solubilized with high concentration of ionic detergent (e.g., 10% sodium deoxycholate), and then the detergent is diluted, so that the disrupted proteins may reassemble, allowing the reassembled protein complexes to be co-immunoprecipitated (Luo et al., 1997).

The surface endocytic zone and endosome pools of N-cadherin (Fig. 1A (1) and (2)) are also supposed to be involved in the plasticity of synaptic structures, and are largely soluble in 1% Triton X-100 by several reasons. First, the surface pools undergo vigorous redistributions by synaptic acitivity (Okamura et al., 2004; Tanaka et al., 2000). These mobile pools were extractable with 1% Triton X-100 in our unpublished observations. Second, the endocytosed N-cadherin is shown to be extracted with 1% Triton X-100/0.1% SDS as detected in western blotting (Tai et al., 2007). Third, the synaptic stimulation-induced trypsin-resistance of N-cadherin was readily detectable in the Triton-soluble fraction as well as in the Triton-insoluble fraction (Fig. 1D). The acquired trypsin-resistance of N-cadherin is a sign of conformational change in response to synaptic activity, and this implies rearrangements of protein–protein interactions (Tanaka et al., 2000).

Thus we reasoned that the determination of protein–protein interactions within the Triton-soluble fraction from synapse-enriched neuronal lysate provides insight into the mechanisms involved in the dynamism of the synaptic structure. There are several advantages by focusing on the Triton-soluble fraction. First, we are able to avoid artificial disruption/reassembly of protein complexes with ionic detergent and its dilution. The intrinsic interactions are directly captured by one-step lysis with Triton X-100. Second, Triton X-100 is a non-ionic detergent and expected to maintain relatively weak protein–protein interactions. The expected disadvantage is that this approach fails to detect the strong protein–protein interactions that involve scaffolding proteins within the PSD.

We used rat hippocampal neurons cultured for 5–6 weeks. Neurons at this stage develop enormous numbers of mature synaptic junctions that are positive for N-cadherin with little contamination by glial cells (Tanaka et al., 2000). Most N-cadherin-positive synaptic puncta cluster at PSD-95-containing postsynaptic densities, a marker of excitatory synapses, but not at GABAergic termini (Benson and Tanaka, 1998). After solubilizing the neurons with 1% Triton X-100, N-cadherin was immunoprecipitated and subjected to SDS–PAGE (Fig. 2A). The bands in the gel specific for anti-N-cadherin antibody but not for control IgG were excised and subjected to in-gel digestion followed by LC–MS/MS analysis (Fig. 2B, Table 1).

We also performed shotgun LC–MS/MS analysis of murine hippocampal extracts in the same buffer conditions. In these

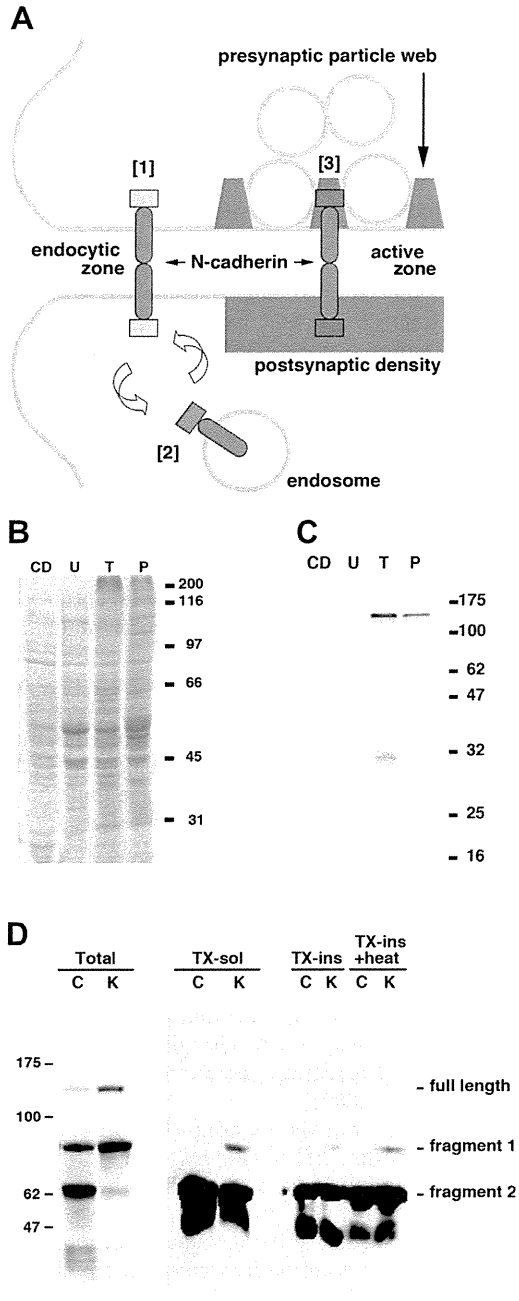

Fig. 1. Solubilization of synaptic membranes with Triton X-100. (A) Schematic representation of synaptic membrane compartments: (1) endocytic zone, (2) intracellular pool, and (3) active zone. Blue bars, N-cadherin; squares (green, orange, purple), N-cadherin-binding proteins. (B) Crude synaptosome fraction isolated from murine hippocampus was sequentially extracted with 20 mM methyl-β-cyclodextrin (CD), 5 M urea (U), 1% Triton X-100 (T), and SDS-sample buffer (P), followed by SDS–PAGE and Coomassie Brilliant Blue staining. (C) Western blot of the sequentially extracted synaptosome fractions probed with anti-N-cadherin antibody. (D) N-cadherin acquires resistance to trypsin upon synaptic stimulation both in Triton-soluble and -insoluble fractions. Unstimulated (lanes C) and stimulated (lanes K) neuron cultures were treated with trypsin (0.1%, 10 min) first and then harvested directly in SDS–PAGE sample buffer (Total), or in 1% Triton X-100-containing buffer for extraction (TX-sol). The Triton-insoluble pellet was resuspended in urea-containing SDS–PAGE sample buffer at room temperature (TX-ins) or at 96 °C (TX-ins + heat), and subjected to western blot. The protected cytoplasmically disposed fragments of partially digested molecules (fragment 1 and 2) as well as intact molecules (full-length) were detected with an antibody recognizing the intracellular domain of N-cadherin. In total neuronal lysates, stimulation (K) induced the increment of the protected full-length N-cadherin and the partially protected fragment 1. In Triton-treated lysates, full-length molecule was not detectable, but the partially protected fragment 1 was increased after the synaptic stimulation.

experiments, specific binding proteins were identified by subtracting control IgG-bound items from N-cadherin-bound items (Table 2).

3.2. Actin cytoskeleton-associated proteins

In addition to immunoglobulin and N-cadherin, two major bands of about 102 and 97 kDa were co-immunoprecipitated and these were identified as αN- and β-catenins, respectively (Table 1, band 7–8). The carboxyl-terminus of N-cadherin is known to be linked to actin cytoskeleton bridged with β- and α-catenins as well as through interactions with various actin-binding proteins such as spectrins (Nelson et al., 1990; Pradhan et al., 2001) and actinins (Knudsen et al., 1995; Nieset et al., 1997). Our results confirmed this as band 2 contained abundant α- and β-spectrins and band 7 contained α-actinin-4 (Table 1). It should be noted that spectrins showed some non-specific binding to the control IgG. However, the intensity of band 2, which mainly contained spectrins, was much higher for N-cadherin than the control IgG (Fig. 2), suggesting that the binding was at least in part specific.

In the shotgun analyses, we identified α- and β-subunits of Na^+/K^+-ATPase (Table 2). In epithelial cells Na^+/K^+-ATPase is known to link plasma membrane to the cortical actin filament network through ankyrin and spectrins (Koob et al., 1988; Morrow et al., 1989; Nelson and Veshnock, 1987). More directly, McNeill and colleagues have demonstrated that uvomorulin (E-cadherin) recruits Na^+/K^+-ATPase and spectrin to the basolateral membrane in a cytoplasmic domain-dependent manner (McNeill et al., 1990). We could not determine whether the linkage of N-cadherin to Na^+/K^+-ATPase exists in neurons or only in glial cells because Na^+/K^+-ATPase was only found in hippocampal extracts and not in cultured neuronal extracts. We also found α-integrin in band 5 (Table 1). A transmembrane cell adhesion molecule, α-integrin, forms a heterodimer with β-integrin, which in turn binds to α-actinin (Otey et al., 1990). Taken together, N-cadherin anchors the cortical actin-associated network involving α-actinin and spectrins, which bridge to other membrane anchor molecules such as integrins and Na^+/K^+-ATPase (Fig. 3A).

3.3. Intermediate filament-associated proteins

Plakoglobin (also known as junction plakoglobin or γ-catenin) was originally identified as a desmosome component, where it can bind to the cadherin family member, desmoglein I (Mathur et al., 1994). The primary structure of plakoglobin shows a close relationship with β-catenin and, in fact, plakoglobin associates with classic cadherins such as N-cadherin (Sacco et al., 1995). Although plakoglobin can anchor classic cadherins via α-catenin to actin in adherens junctions, it loses this ability when incorporated into desmosomes. This specificity is achieved by mutually exclusive interactions of plakoglobin with α-catenin and desmosomal cadherins (Chitaev et al., 1998). On the other hand, the binding of β-catenin and plakoglobin to the common N-cadherin cytoplasmic domain in a mutually exclusive manner (Nathke et al., 1994) raises the possibility of competition between these proteins for N-cadherin. For example, high expression of exogenous plakoglobin can efficiently displace endogenous β-catenin from adherens junctions (Sacco et al., 1995; Salomon et al., 1997). Similarly, in plakoglobin-knockout mice, β-catenin is incorporated into desmosomes, which are normally devoid of this protein (Bierkamp et al., 1999).

In the present study, in addition to β-catenin (band 8), plakoglobin was simultaneously bound to N-cadherin (band 10) (Table 1). This finding was confirmed in hippocampal shotgun analysis (Table 2). Furthermore, desmoplakin, which serves as a bridge

Table 1
Proteins identified in SDS-gel bands with applied N-cadherin-immunoprecipitate.

Description	Mascot score	Accession[a]	Confirm[b]
Band 1			
DYHC1; cytoplasmic dynein 1 heavy chain 1	98.26	729378	Ref.
Band 2			
SPTA2; spectrin alpha chain, brain	190.27	17380501	Ref.
Non-erythrocyte beta-spectrin	10.15	13430206	Ref.
Sptbn1 protein	10.14	60422766	Ref.
Band 3			
Protein for IMAGE:9026960; sperm-associated antigen 9	28.20	197245955	CR
Sperm-associated antigen 9	10.16	157819127	CR
Band 4			
Clathrin, heavy chain (Hc)	180.28	9506497	NS
CADH2; cadherin-2; neural cadherin; N-cadherin; CD325	50.26	13431334	–
Protein for IMAGE:9026960; sperm-associated antigen 9	10.23	197245955	CR
Similar to tripartite motif protein 33	20.22	62644337	CR
Band 5			
rCG36779; ARVCF	50.27	149019791	Ref.
CADH2; cadherin-2; neural cadherin; N-cadherin; CD325	30.24	13431334	–
Amphiphysin	10.18	11560002	ND
Integrin alpha chain	10.12	56393	ND
Catenin (cadherin-associated protein), alpha 2	10.07	157817081	Ref.
Pumilio homolog 1	10.10	157822487	ND
Band 6			
DDB1; DNA damage-binding protein 1	50.32	81868411	NS
Catenin (cadherin-associated protein), alpha 2	140.28	157817081	Ref.
Catenin (cadherin-associated protein), alpha 1, 102 kDa	34.23	55742755	Ref.
Damage-specific DNA-binding protein 1	10.17	149062405	NS
Phosphorylase kinase, beta	10.16	62079039	ND
Band 7			
Catenin (cadherin-associated protein), alpha 1, 102 kDa	320.35	55742755	Ref.
Catenin (cadherin-associated protein), alpha 2	200.29	157817081	Ref.
B39529 cadherin-associated protein, 102 K - rat (fragments)	10.24	92036	Ref.
Similar to catenin delta-2 (NPRAP) (neurojungin)	10.24	109464562	Ref.
rCG38081 (tRNA-binding, unknown function)	8.12	149055468	ND
Alpha-actinin 4	10.16	6636119	Ref.
Beta-catenin	10.16	46048609	Ref.
Band 8			
Beta-catenin	338.34	46048609	Ref.
Catenin (cadherin-associated protein), alpha 1, 102 kDa	30.22	55742755	Ref.
Catenin (cadherin-associated protein), alpha 2	22.15	157817081	Ref.
Cadherin-associated protein, 102 K (fragments)	10.24	92036	Ref.
Valosin-containing protein	10.20	17865351	ND
Proteasome (prosome, macropain) 26S subunit, non-ATPase, 2	10.23	72255509	ND
Band 9			
Beta-catenin	148.29	46048609	Ref.
Catenin (cadherin-associated protein), alpha 1, 102 kDa	20.20	55742755	Ref.
Cadherin-associated protein, 102 K (fragments)	10.22	92036	Ref.
Catenin (cadherin-associated protein), alpha 2	30.18	157817081	Ref.
Band 10			
Heat shock protein 90, alpha (cytosolic), class A member 1	30.26	28467005	ND
Junction plakoglobin	50.28	41529837	Ref.
Beta-catenin	50.25	46048609	Ref.
TNF-receptor-associated protein 1	10.22	84781723	DN
Annexin A2	10.17	9845234	ND
Dsp protein; desmoplakin	10.15	67678070	Ref.
Band 11			
Grp75 (DnaK, HSP9)	30.19	1000439	ND
HNRPM; heterogeneous nuclear ribonucleoprotein M	40.21	71152132	ND
DnaK-type molecular chaperone hsp72-ps1	50.19	347019	ND
Beta-catenin	10.21	46048609	Ref.